ADVANCED ENERGY MATERIALS
www.advenergymat.de

Water-Soluble Inorganic Binders for Lithium-Ion and Sodium-Ion Batteries

Shivam Trivedi, Venkat Pamidi, Sebastian Pinto Bautista, Farra Nur Aliah Shamsudin, Marcel Weil, Prabeer Barpanda, Dominic Bresser, and Maximilian Fichtner**

Inorganic materials form an emerging class of water-soluble binders for battery applications. Their favourable physicochemical properties, such as intrinsic ionic conductivity, high thermal stability (>1000 °C), and compatibility to coat a diverse range of electrode materials make them useful binders for lithium-ion and sodium-ion batteries. Li and Na containing phosphates and silicates are attractive choices as multifunctional inorganic aqueous binders (IABs). This review discusses these binders' structural, thermal, and ionic properties, followed by exploiting their ionically conducting nature for all-solid-state batteries. Subsequently, the application of these compounds as binders and surface coating agents for different anodes and cathodes in lithium-ion and sodium-ion batteries is discussed. Eventually, a first evaluation of their environmental impacts and economic aspects is presented as well.

1. Introduction

Batteries have revolutionized our life by enabling the use of portable electronic devices (e.g., laptops, smartphones, and power tools) and eco-friendlier transportation in the form of electric vehicles. As such they are considered a key element for the transition to a carbon-free and sustainable economy and a reduced dependence on fossil fuels. Lithium-ion batteries (LIBs) have proven to be the benchmark for electrochemical energy storage in the past three decades, but they commonly employ several critical and expensive raw materials such as cobalt and lithium.[1–3] Owing to the high abundance, wider geographical distribution, and low cost of sodium precursors, sodium-ion batteries (SIBs) have recently emerged as the next high-performance battery technology.[4,5] They benefit from an analogous overall charge storage mechanism and the extensive knowledge gained on LIBs. Given the general differences in energy and power density, operational temperature range, and potential cost, these two battery technologies are considered complementary to each other.[3] For both, various electrode materials and electrolytes have been explored with the aim of improving their performance.[6–17] However, the role of the binder is frequently underestimated, as it accounts only for a rather small fraction of electrode composition and cell and, hence, the overall cost of the final battery cells. Nonetheless, the binder has an important impact beyond its primary role of holding together the electrode components, i.e., the active material particles, the conducting additive, and the current collector (**Figure 1a**) while ensuring suitable mechanical properties of the electrodes. The choice of the binder also affects the formation and composition of the solid electrolyte interface (SEI), the charge transfer within the electrode and across the electrode–electrolyte interface, the wetting behavior of the electrodes, as well as the sustainability and cost of the final battery cell.[18–23] Polyvinylidene difluoride (PVdF) for instance, as the state-of-the-art binder for lithium-ion and sodium-ion cathodes shows very good binding properties for a wide range of materials combined with high chemical resistance and electrochemical stability.[24,25] Moreover it absorbs liquid electrolytes (LEs), which enables a high ionic transport within the electrode.[19,26-28] Despite these favorable features, however, it also faces challenges.[29] First and foremost it

S. Trivedi, V. Pamidi, S. P. Bautista, M. Weil, P. Barpanda, D. Bresser, M. Fichtner
Helmholtz Institute Ulm (HIU)
89081 Ulm, Germany
E-mail: shivam.trivedi@kit.edu; m.fichtner@kit.edu
S. P. Bautista, F. N. A. Shamsudin, M. Weil
Institute for Technology Assessment and Systems Analysis (ITAS)
Karlsruhe Institute of Technology
76021 Karlsruhe, Germany
P. Barpanda, M. Fichtner
Institute of Nanotechnology (INT)
Karlsruhe Institute of Technology (KIT)
76021 Karlsruhe, Germany
P. Barpanda
Faraday Materials Laboratory (FaMaL)
Materials Research Centre
Indian Institute of Science (IISc)
Bangalore 560012, India
D. Bresser
Karlsruhe Institute of Technology
76021 Karlsruhe, Germany

The ORCID identification number(s) for the author(s) of this article can be found under https://doi.org/10.1002/aenm.202303338

DOI: 10.1002/aenm.202303338

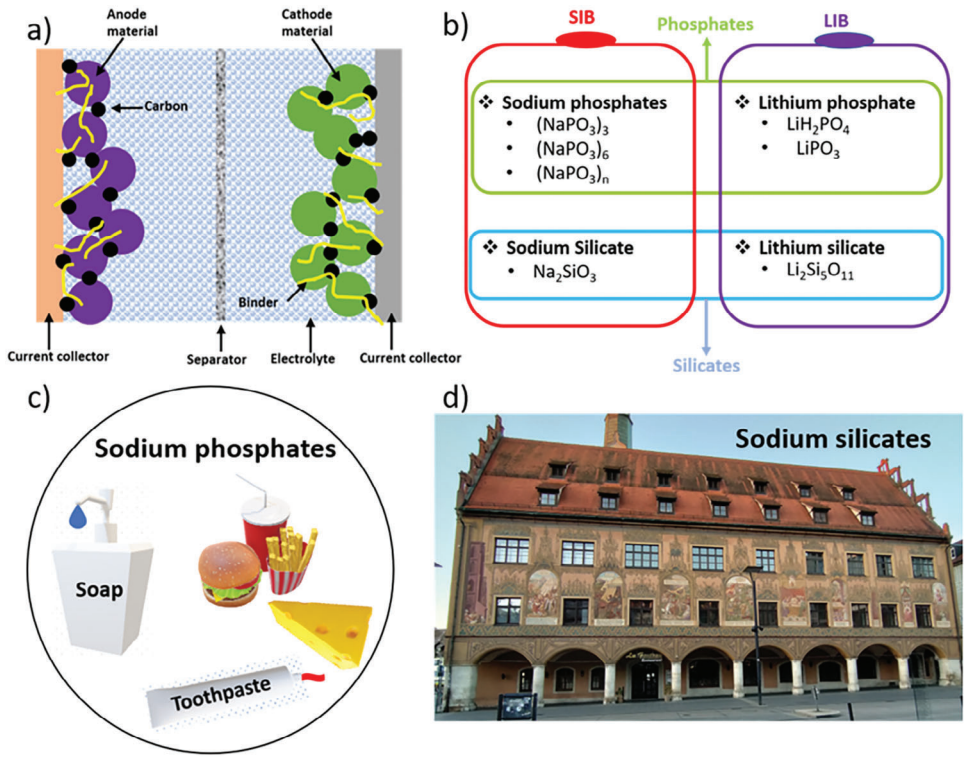

Figure 1. a) Schematic of a Li-ion/Na-ion battery with a focus on the electrode composition, including the active material, conductive carbon, and the binder. b) Classification of inorganic aqueous binders (IABs), c) General applications of sodium phosphates in everyday life items. d) Photograph of an exemplary application of sodium silicate in buildings (inspired by ref. [40]).

necessitates the usage of *N*-methyl pyrrolidone (NMP) as a processing solvent, which is rather expensive, harmful, and raises severe environmental concerns, thus requiring stringent protocols for working with it and the eventual disposal and recycling.[30,31] Additionally, PVdF is characterized by a highly insulating nature, which further worsens the occurrence of improperly dispersed conductive carbon. The ionically insulating nature of binders such as PVdF is also a serious bottleneck in the case of all-solid-state batteries (ASSBs) that suffer from high interfacial resistance.[32,33]

To mitigate these issues, (fluorine-free) water-soluble (aqueous) binders have been intensively investigated in recent years—not least triggered by the great success of lithium-ion anodes.[31,34,35] This would eliminate the need for harmful NMP, and allow for substantial advantages in terms of sustainability and cost owing to the potential reduction of the drying time. In particular, organic aqueous binders such as carboxymethyl cellulose (CMC), styrene-butadiene rubber (SBR), polyacrylic acid (PAA), polyvinyl alcohol (PVA), and alginate (ALG) have attracted great attention for both anodes and cathodes. Accordingly, several review articles have summarized the properties and electrochemical performance of these binders.[18,31,34–39]

In contrast, inorganic aqueous binders (IABs) have attracted significantly less attention so far despite potential advantages, as summarized and highlighted in the following sections of this—to the best of our knowledge—first review article on IABs.

2. Inorganic Aqueous Binders

Inorganic binders are an emerging class of aqueous binders and have only been sparsely investigated until now. Nonetheless, their commonly higher thermal stability, potential flame-retardant properties, and the possibility to use abundant elements warrant increasing efforts to explore their potential use in rechargeable batteries.[40–45] The IABs discussed in this review comprise sodium- and lithium-containing phosphate and silicate salts (Figure 1b). In this section, we will briefly reflect on the background, and summarize the relevant physicochemical and mechanical properties of these IABs.

2.1. Background

Sodium phosphates are well-known food additives in many countries of the world, including Canada, Europe, the United States, and Australia. They are employed in a variety of foods as emulsifiers, thickening, and pH control agents, as well as preservatives (Figure 1c).[46,47] In addition, they are also used in soaps and detergents due to their water-solubility and basicity, enabling the saponification of grease and oil.[48] Most of these phosphate monomers are linked with ionic bonds yielding oligomeric or even polymeric chains. Apart from phosphates, alkali polysilicates (also known as "water glass") for instance sodium silicate have been known to the foundry industry as a sand binder since 1950 for the production of molding and core sands.[49,50] Generally, alkali phosphates and silicates are also utilized in

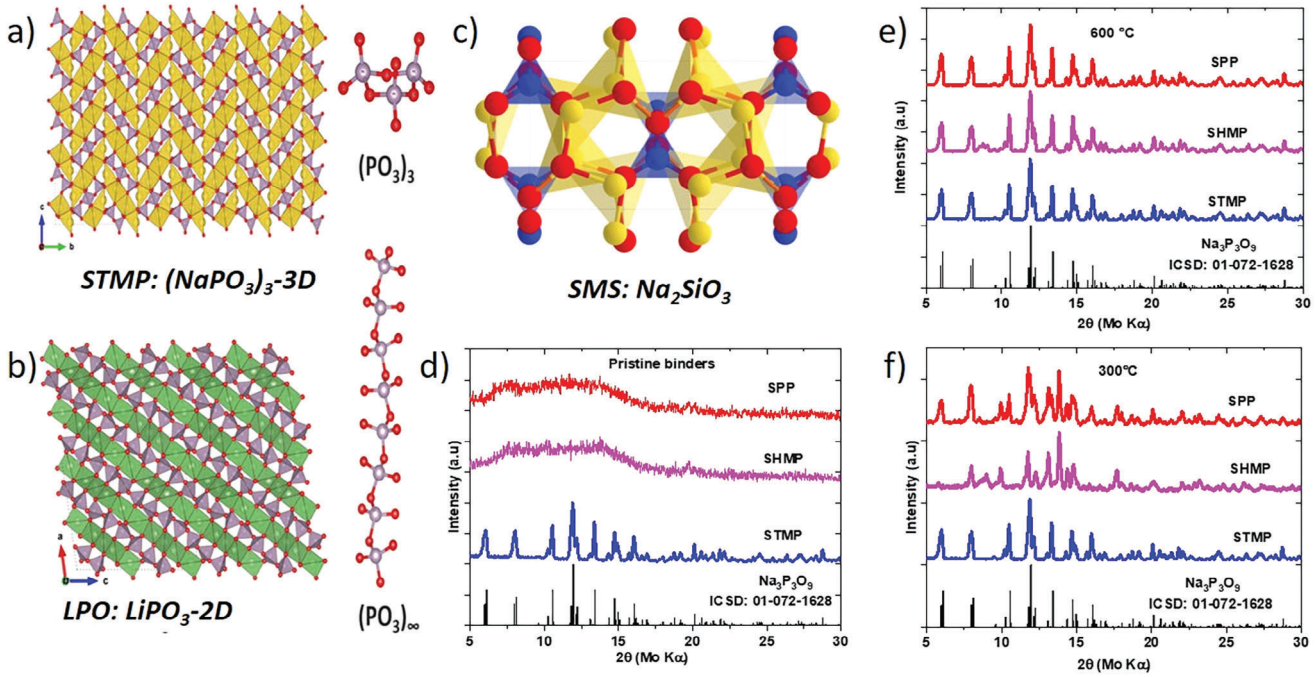

Figure 2. Properties of IABs: a) Crystal structure of sodium trimetaphosphate (STMP: $(NaPO_3)_3$). b) Crystal structure of lithium phosphate (LPO: $LiPO_3$). c) Crystal structure of sodium metasilicate (SMS: Na_2SiO_3), produced from Materials Project database. d) XRD patterns of pristine STMP: $(NaPO_3)_3$, SHMP: $(NaPO_3)_6$, and SPP: $(NaPO_3)_n$. e) XRD patterns of STMP, SHMP, and SPP after heating at 600 °C. f) XRD patterns of STMP, SHMP, and SPP after treating with water followed by drying and heating at 300 °C. a,b,d–f) Reproduced with permission.[43] Copyright 2022, Royal Society of Chemistry.

impermeable paint coatings and refractories (Figure 1d).[51] In this context, their favorable properties such as water solubility, high adhesion strength, and thermal stability have been leveraged for applications such as refractory adhesives, paints, and cement additives.[49,52–54]

To the best of our knowledge, the first instance of the application of silicate-based IABs for battery electrodes was acknowledged in the year 1996.[55] The inventors utilized lithium polysilicate (LPS: $Li_2Si_5O_{11}$) as a binder for graphite anodes and $LiCoO_2$ cathodes for lithium-ion cells, which was also patented by "Mitsubishi Chemical Corporations, (Japan)" in the year 1999. Later in 2011, another patent claimed several inorganic compounds including metal phosphates and silicates as prospective binders for battery electrodes.[41] The inventors claimed several advantageous properties, including ionic conductivity, and proposed them as suitable binders for LIBs and SIBs. However, no clear data were provided neither concerning the given properties nor their eventual electrochemical performance as battery electrode binders. Also, no follow-up research was reported for over a decade and the full potential of these binders was not realized until recently.[40,42,43,56–58]

2.2. Physicochemical Properties

Sodium phosphate salts consist of Na^+ cations and PO_4^{3-} anions. The network is dominated by anionic linkages existing together as a polymeric network. Sodium phosphate derivatives $(NaPO_3)_x$: trimer (sodium trimetaphosphate: STMP, $n = 3$, **Figure 2a**), hexamer (sodium hexametaphosphate: SHMP $n = 6$), and polymer (sodium polyphosphate: SPP, $x = n$) along with lithium phosphates (LHPO: LiH_2PO_4 and LPO: $LiPO_3$, Figure 2b) were investigated for their physicochemical properties and as potential binders with different electrode materials. In addition, sodium metasilicate (SMS: Na_2SiO_3, Figure 2c) and lithium polysilicate (LPS: $Li_2Si_5O_{11}$) were also explored.[43]

2.2.1. Structural Properties

Among the three sodium phosphates (STMP, SHMP, and SPP), only STMP exhibits a crystalline nature (Figure 2d). It is built with an isolated $(P_3O_9)^{3-}$ cluster network connected via NaO_5 polyhedra.[43,59] The sodium atoms are fivefold coordinated with oxygen atoms. It has two different Na atoms: Na1 and Na2. $Na1O_5$ and $Na2O_5$ polyhedra are connected diagonally to each other through a common edge, generating a zig-zag pathway for Na^+ diffusion. It has distinct inter and intra connections of $Na1O_5$ and $Na2O_5$ polyhedra, which allow the 3D diffusion of Na^+ (Figure 2a). SHMP and SPP are amorphous in nature (Figure 2d). Upon heating, both SHMP and SPP crystallize into STMP at 600 and 300 °C, respectively (Figure 2e). Both SHMP and SPP show a chain-like PO_3 structure. The structure of lithium phosphate ($LiPO_3$) is based on LiO_4 tetrahedra and $(PO_3)_\infty$ chains (Figure 2b).

When getting in contact with water, chain-type phosphates (SHMP and SPP) rapidly hydrolyze resulting in the formation of hydrolyzed products of the respective compounds and crystallize into STMP on thermal treatment at 300 °C (Figure 2f).[60] Sodium metasilicate (SMS: Na_2SiO_3) is polymeric in nature,

Table 1. Summary of the binders' properties. Data were acquired from references.[24,43,45,61,87,88]

Binder	Nature of binder	Thermal stability		Adhesion strength	Ionic conductivity [S cm^{-1}]	
		Melting point	Stable up to		60 °C	200 °C
STMP	Inorganic	600 °C	>1000 °C	6.2 N	6.1×10^{-11}	1.2×10^{-7}
					4.7×10^{-10}	5.0×10^{-6}
SHMP	Inorganic	628 °C	>1000 °C	6.3 N	–	–
SPP	Inorganic	555 °C	>1000 °C	6.6 N	4.2×10^{-10}	2.4×10^{-6}
SMS	Inorganic	1088 °C	>1000 °C	9 N	5.3×10^{-10}	1.5×10^{-7}
LHPO	Inorganic	-	200 °C	-	1.6×10^{-8}	2×10^{-5}
LPO	Inorganic	656 °C	>1000 °C	-	3.7×10^{-10}	4×10^{-5}
LPS	Inorganic	-	>1000 °C	-	2.9×10^{-10}	1×10^{-7} (160 °C)
PVDF	Organic	160-180 °C	400 °C	1.6 N	–	–
CMC	Organic	220 °C	260 °C	4.2 N	1.1×10^{-10} (100 °C)	1.4×10^{-8}
PAA	Organic	116 °C	400 °C	-	8.7×10^{-10}	2.5×10^{-6}

consisting of corner-shared SiO_4 tetrahedra, which are interconnected three-dimensionally by NaO_4 tetrahedra. It crystallizes in the orthorhombic system. Further details on the structural and mechanical properties are reported in the literature.[61–63] Both STMP and SMS possess 3D diffusion pathways for Na^+ favoring an efficient ion transport when used as electrode binder. The elaborate structural analysis of these compounds has been investigated by us previously.[43]

2.2.2. Thermal Properties

The thermal stability of binders is one of the most important parameters for the operational safety of batteries. Conventional PVdF binder has a low melting point of ≈160 °C.[24] Therefore, the films coated with PVdF are dried below this temperature. Nevertheless, even drying below its melting point can alter its physical and chemical properties. PVdF has four different phases (α, β, Υ, and δ), which transform into one another depending on the processing temperature.[24] In principle, drying at less than 100 °C, leads to a mixture of the α and β phase, while the formation of the Υ phase is observed at temperatures beyond 155 °C. These phases are also influenced by active materials and conductive additives. The characteristics of binders are also influenced by their molecular weight. In short, it is very challenging to optimize and control the temperature-dependent phases of PVdF to achieve an enhanced electrochemical performance.

An additional issue when using PVdF originates from the temperature-induced decomposition in the case of a thermal breakdown of the SEI which starts at ≈100–140 °C, followed by a reaction between the (partially) lithiated graphite (Li_xC_6) and the electrolyte resulting in a further temperature increase to ≈210–230 °C.[64,65] This is seen as an exothermic reaction via differential scanning calorimetry (DSC) and a small mass loss as observed in thermogravimetric analysis (TGA).[66] Above 300 °C, eventually, the PVdF binder undergoes an exothermal defluorination reaction in contact with the lithiated graphite (Li_xC_6) and metallic lithium resulting in the formation of H_2 and LiF.[65,66] In fact, even at much lower temperatures, PVdF loses its mechanical properties, leading to a degradation of the original electrode structure. The summary of the binders' properties is given in **Table 1**.

Batteries should be able to withstand a wide range of temperatures (−20 to +60 °C) for commercial applications.[67] High temperatures (≈50 °C) and high current rates can significantly degrade the battery performance and also promote thermal runaway reactions leading to disastrous effects.[68,69] To address this issue, the introduction of binders with a higher thermal stability appears as a suitable approach. Efforts have been made to utilize thermally stable binders to fabricate safe batteries.

Park and co-workers, for instance, showed that PAA-based graphite electrodes exhibited a reduced heat evolution compared to CMC-SBR and PVdF-based electrodes.[72] The highest heat evolution was observed in the case of PVdF binder due to its lower thermal stability, weak adhesion, and swelling in LEs.[72,73] In contrast, PAA binder acts as a protective film inhibiting direct contact between graphite and LE, consequently suppressing the delithiation at high temperatures.[74] Nevertheless, such organic binders still decompose at temperatures of ≈400 °C,[75] leaving space for further improvement—especially when it comes to elevated temperatures of over 600 °C in the case of thermal runaway. Therefore, binders with a further increased thermal stability would be beneficial for safety reasons and IABs appear particularly suitable in this regard owing to their excellent thermal stability.

Zhou and co-workers for instance studied ammonium polyphosphate (APP: $(NH_4.PO_3)_n$) as a binder for sulfur cathode in Li–S batteries.[44] APP is known to be an effective flame retardant. Therefore, to test its effectiveness in capping the flammability of sulfur electrodes, PVdF and APP-based sulfur electrodes were exposed to direct flame until ignition. The specific burning time was calculated to be 519 sg^{-1} with PVdF binder. This was significantly reduced to 289 sg^{-1} in the case of APP. APP melts and converts to a highly cross-linked polyphosphoric acid at ≈300 °C. This acts as a physical barrier to heat and it remains stable until 550 °C, before dehydrating to P_4O_{10}.[76,77]

Further improvement was realized by introducing IAB for $Na_{0.7}Mn_{0.7}Mg_{0.1}O_2$ (NMO) cathodes and graphite anodes for SIBs and LIBs respectively.[43] IABs possess a very high thermal stability up to 1000 °C with weight loss of <2% in sodium

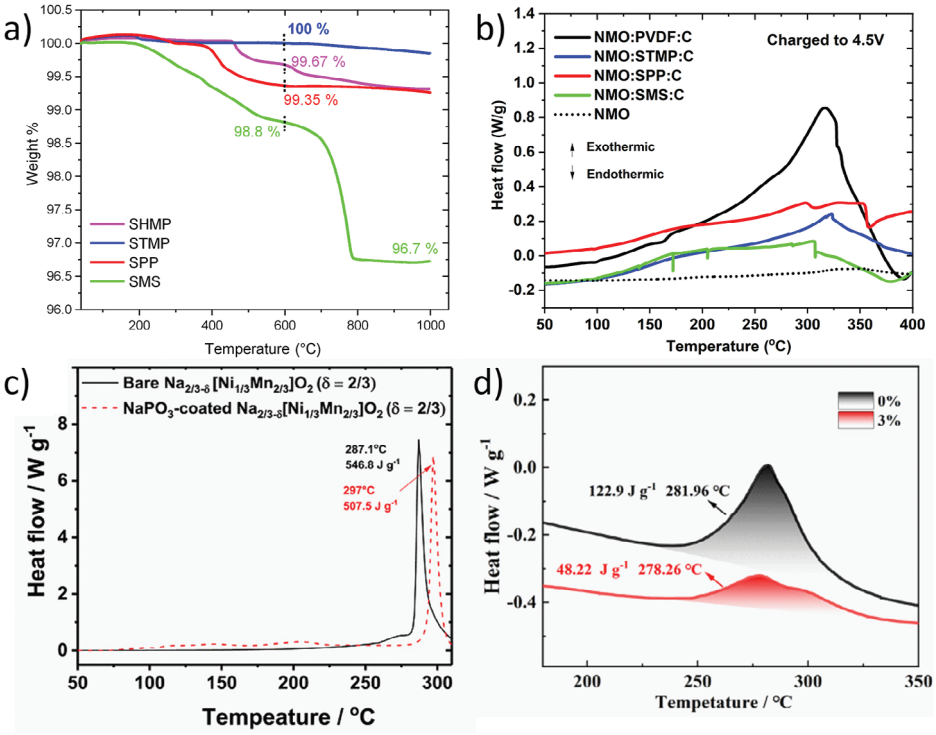

Figure 3. Thermal properties: a) TGA of sodium phosphates (STMP: $(NaPO_3)_3$, SHMP$(NaPO_3)_6$, and SPP: $(NaPO_3)_n$)) and sodium meta silicate (SMS: Na_2SiO_3) binders. b) DSC of desodiated $Na_{0.7}Mn_{0.9}Mg_{0.1}O_2$ (NMO) electrode with PVdF, STMP, SPP, and SMS as binders. a,b) Reproduced with permission.[43] Copyright 2022, Royal Society of Chemistry. c) DSC of desodiated bare and $NaPO_3$-coated $Na_{2/3-\delta}(Ni_{1/3}Mn_{2/3})O_2$ ($\delta = 2/3$) cathode. Reproduced with permission.[70] Copyright 2018, Wiley-VCH. d) DSC of the bare and SMS-coated P2-$Na_{0.67}Fe_{0.5}Mn_{0.5}O_2$ (NFMO) cathode in a desodiated state. Reproduced with permission.[71] Copyright 2021, Elsevier.

phosphate binders and <4% in the case of SMS owing to the loss of surface groups (**Figure 3a**). NMO-IAB electrodes exhibited significantly lower heat release in charged (de-sodiated) state as compared to PVdF-based electrode (Figure 3b). Similar effects were also observed in the case of discharged (lithiated) graphite anode.[43] Moreover, the NMO-STMP electrodes did not lose adhesion and maintained physical integrity even after thermal treatment at 600 °C owing to the high thermal stability of IAB. In another report by Jo et al.,[70] $NaPO_3$ coating on P2-$Na_{2/3}(Ni_{1/3}Mn_{2/3})O_2$ cathode delayed the formation of Mn_3O_4 and oxygen evolution from the lattice leading to improved thermal stability of the material as compared to bare electrode in the desodiated state (Figure 3c). Similar study with SMS-coated P2-$Na_{0.67}Fe_{0.5}Mn_{0.5}O_2$ (NFMO) cathode showed ≈2.5 times less heat evolution as compared to bare sample in desodiated state (Figure 3d).[71]

It is therefore suggested that IAB binders can counter exothermic reactions by acting as a heat sink and preventing thermal runaways in the battery. However, further investigations would be needed to evaluate the thermal and safety features of these binders.

2.2.3. Adhesive properties

A high adhesion strength is a fundamental prerequisite to maintain suitable mechanical properties and ensure a good electronic contact within the electrode. Traditionally, electrode slurries are processed in a suitable solvent by initially dissolving the binder and subsequently adding the active material and the conductive carbon. This composite slurry mixture is coated on a suitable metallic substrate (commonly, copper or aluminum foils) and subsequently dried to remove the solvent.

PVdF interacts with the electrode material via weak van der Waals forces.[24] Such relatively weak interaction might cause contact issues during cycling, especially if the active material particles undergo pronounced volume changes during cycling. Additionally, under alkaline conditions, PVdF tends to form a gel which potentially affects the uniformity and electrode morphology (particularly in the case of alkaline cathodes).[24,78] Other organic polymers such as CMC, PAA, and PVA possess abundant carboxyl and hydroxyl functional groups that allow for a stronger interaction with the electrode material. These functional groups are able to engage in hydrogen and covalent bonding with surfaces, depending on the nature of the active material.[35,79–82]

Commonly, the binders undergo two steps: initially, it wets the substrate and the electrode material in the dissolved state, before it organizes and hardens during drying.[36] The eventual distribution of the binder and the overall electrode microstructure depends on the initial mixing and dispersion, the degree of reorganization during drying, the speed of the solvent evaporation, and the interaction of the binder with the conductive carbon and the active material particles.[83,84] Consequently, these factors also determine the surface area and porosity of the electrode as well

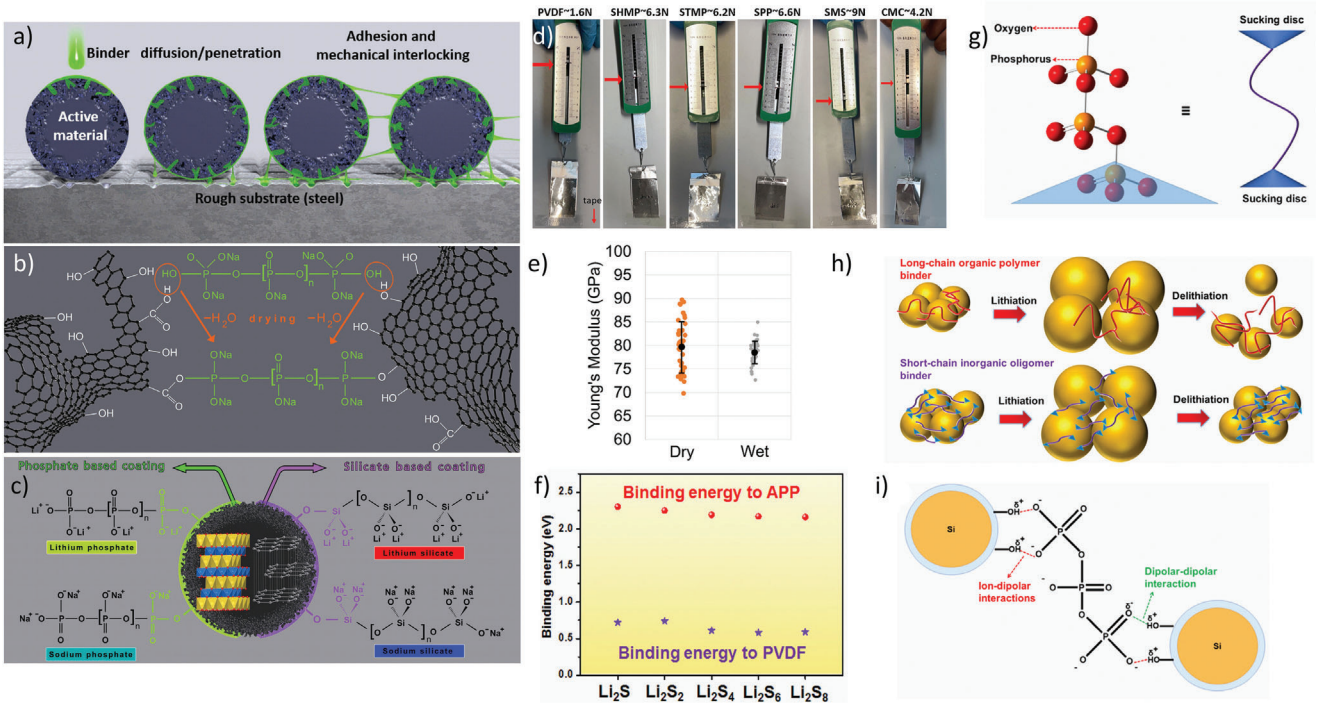

Figure 4. Binding mechanisms and mechanical properties of different inorganic aqueous binders (IAB). a) Binding mechanism of IAB on a rough surface (e.g., steel) by mechanical interlocking. b) Binding mechanism of IAB with hard carbon. c) Binding mechanism of IAB utilizing the phosphate and silicate groups of surface coatings for adhesion. d) Adhesion strength of different binders as measured by peel tests. Under review.[45] e) Effect of electrolyte wetting on the physical properties of SMS binder. Reproduced with permission.[40] Copyright 2021, Nature. f) Binding strength of ammonium polyphosphate (APP) and PVdF with various Li–S species. Reproduced with permission.[44] Copyright 2018, American Chemical Society. g) Molecular structure of potassium triphosphate (PTP) binder. h) Schematic representation of the lithiation/delithiation process in silicon anodes using a long-chain polymer and short-chain inorganic oligomer. i) Mechanism of interfacial reactions between PTP and Si particles. Reproduced with permission.[58] Copyright 2021, American Chemical Society.

as the eventual binding strength. In the presence of chemical binding sites, bond formation (covalent/ionic/metallic) and electron exchange may occur. Therefore, the presence of functional groups in the binding agent may substantially add to achieving strong adhesion. To enable a strong adhesion with the smooth current collectors several binder designs have been developed. Very recently Wang and co-workers developed spider-silk like flexible binder prepared by cross-linking poly(urethane-urea) to PAA and utilized it for flexible LIB.[85]

Several binding theories and mechanisms have been elaborated in the previous literature.[36,84]

Nonetheless, the binding mechanism of IABs is still ambiguous and has not been completely understood. Based on the current knowledge, mechanical interlocking between substrate, active material, and binder could be one binding mechanism.[36] This is usually prominent in materials with intrinsic surface roughness (e.g., hard carbons) adhering to rough and irregular surfaces such as steel (**Figure 4a**). This mechanical interlocking can be compared to the adhesion of glue on the porous surface of wood. According to another proposed mechanism, IABs hydrolyze and develop OH^- groups during aqueous processing, which connect to the surface groups of the active material via condensation reaction during heating, thus forming a new bond.[42,43,56] This adhesion mechanism could be more prominent in materials with surface functionalities such as hydroxyl, and carboxyl groups (Figure 4b). In materials with a few or no functional surface groups as for instance, graphite and layered oxides, the application of IAB surface coatings on these active materials does not only help to enhance the adhesion, but also leads to improved interfacial properties, reducing side reactions, promoting ionic diffusion and stabilizing the SEI. Following this strategy, phosphate and silicate functionalities are in general helpful for phosphate and silicate-based IABs respectively (Figure 4c, also discussed in Section 4.1). In a recent report by Wang et al.,[56] the authors proposed an autohesion mechanism, where the binder and active material particles get in tight contact, forming strong bonds. They investigated silicon anodes with a lithium metasilicate (LMS: Li_2SiO_3) binder and suggested the formation of covalent and hydrogen bonding between —OH and SiO_2 groups on the surface of LMS and silicon. In summary, one or more binding mechanism could be occurring simultaneously, calling for more in-depth studies.

An investigation of the binding strength showed that SMS provides a very high adhesion strength of 9 N as compared to only 1.6 N and 4.2 N with PVdF and CMC, respectively. Sodium phosphate binders also exhibited a high adhesion strength of ≈6 N (Figure 4d).[45] Preferably a binder should remain rigid and not soften in contact with an electrolyte. Ransil and co-workers used the nanoindentation technique to evaluate the effect of electrolyte wetting on the physical properties of binder films.[40] SMS was found to be two orders of magnitude stiffer than the PVdF. Also, it does not soften when exposed to LE (Figure 4e), whereas PVdF

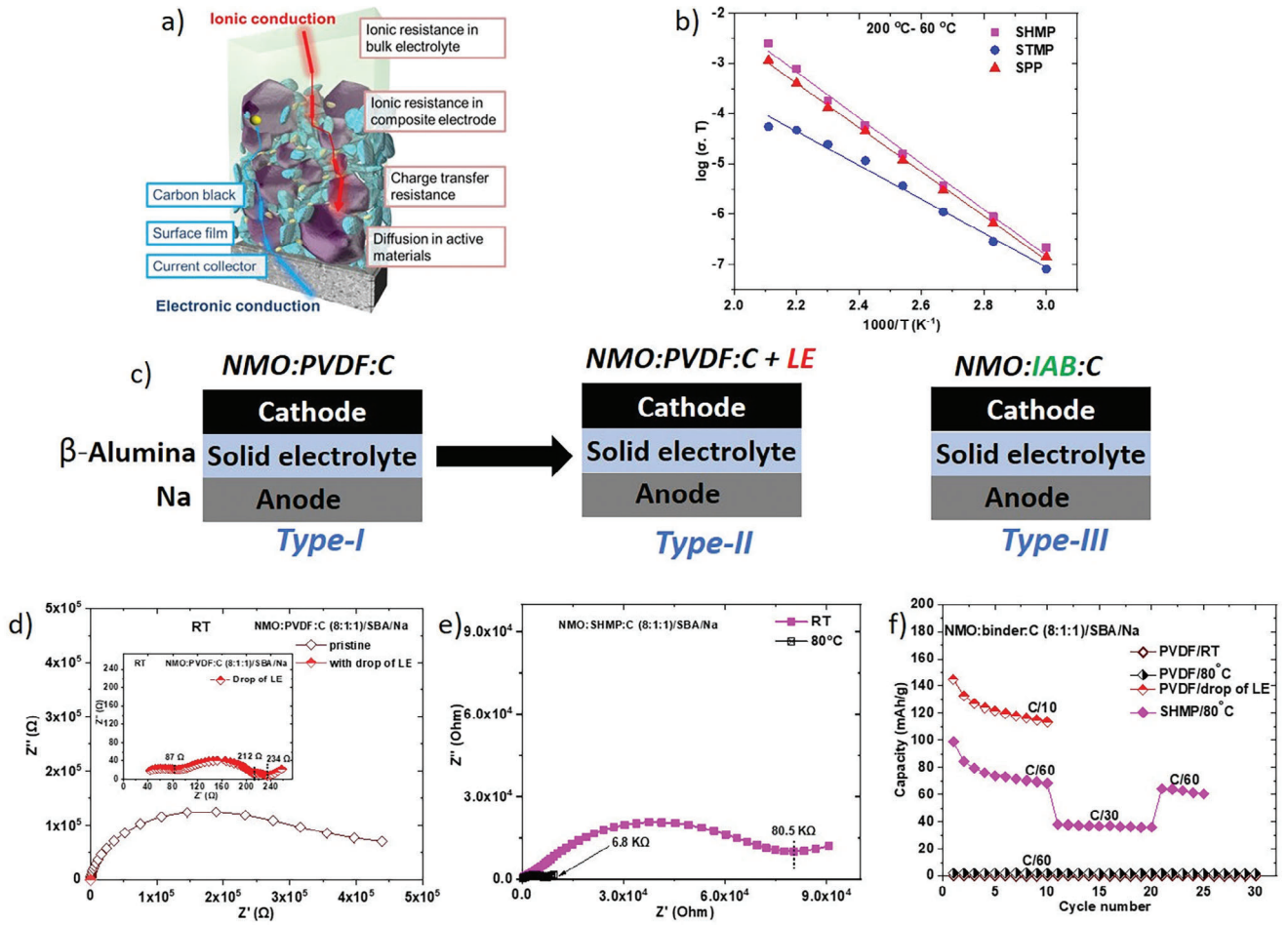

Figure 5. a) Schematic of the composite electrode in LIB. Reproduced with permission.[89] Copyright 2016, Nature. b) Arrhenius plots (ionic conductivity) of sodium phosphate binders. Reproduced with permission.[43] Copyright 2022, Royal Society of Chemistry. c) Schematic of Type I-III solid-state battery (SSB). d) Impedance of $Na_{0.7}Mn_{0.9}Mg_{0.1}O_2$-PVdF SSB with and without liquid electrolyte (LE). e) Impedance of inorganic aqueous binder-based SSB at RT and 80 °C. f) Rate capability of different SSBs. d–f) Reproduced with permission.[43] Copyright, 2022, Royal Society of Chemistry.

softens by an additional order of magnitude.[86] SMS maintains Young's modulus of >50 GPa in the presence of electrolyte; a characteristic that might be beneficial for load-bearing structural battery electrodes.[40] In another theoretical study, APP was found to show a strong binding affinity with lithium polysulfides, inhibiting the shuttling effect of polysulfide anions.[44] APP can induce binding energies in the range of 2.16–2.30 eV with different lithium polysulfides, being much higher than PVdF (0.58–0.74 eV, Figure 4f). This high binding strength was attributed to the large polarization strength in the P—O chain. Among the high energy density electrodes such as silicon, potassium triphosphate (PTP: $K_5O_{10}P_3$) based inorganic binders have been utilized for better adhesion and cyclability (Figure 4g).[58] The abundant P—O^- and P═O bonds of PTP generate strong ion–dipolar and dipolar–dipolar forces with —OH groups on the surface of silicon (Figure 4h,i). The average Young's modulus of the Si-PTP electrode was observed to be 1043 MPa, i.e., much higher than the values determined for Si-PVdF (811 MPa) and Si-CMC (571 MPa) electrodes. This helped the Si-PTP electrodes to withstand the high stress during volume changes upon electrochemical cycling. The adhesion strength of the electrodes was evaluated using PeakForce Quantitative NanoMechanics (atomic force microscope). The average adhesion of the Si-PTP electrode was found to be 10.2 nN and hence, significantly higher than the values recorded for Si-PVdF (7.42 nN) and Si-CMC (6.97 nN) electrodes.

2.2.4. Ionic Conductivity

The implementation of ionically conductive binders would provide a big step toward advanced electrodes for higher energy and power density. Ionic conductivity (IC) within the composite electrode is crucial to shuttle ions between the electrode and electrolyte (**Figure 5a**). Most of the commonly used binders, though are ionically insulating, the IC in the electrode is ensured by incorporation of the LE. This is apparently an issue when considering the preparation of electrodes for all-solid-state batteries (ASSBs).[32,89,90] Therefore, binders with intrinsic IC are needed to bridge this gap. Apart from ASSB, such binders may also be helpful with LEs-based battery in improving power density due to increased charge carrier density. Additionally, ionically

conducting binders can provide ionic transport pathways in case of thicker electrode designs or in the case of insufficient wetting (e.g., with viscous electrolytes such as ionic liquids).[91]

Several research groups have investigated the ionic properties of Na/Li phosphates and silicates. Lithium phosphate (Li_3PO_4), in fact, has been studied as a promising candidate for solid-state electrolytes (SSE). The amorphous phase shows higher IC than its crystalline counterpart (4.2×10^{-18} S cm^{-1}).[92–94] Therefore amorphous thin films with an ionic conductivity of 7×10^{-8} S cm^{-1} (25 °C) have been studied as SSE. Apart from this, it has extensively been utilized for surface coating a wide range of cathode materials to leverage several advantages including IC (detailed in Section 4.3). Despite its ionically conducting nature, its poor water solubility restricts its usage as an aqueous binder. Its sodium counterpart, i.e., Na_3PO_4 has also been reported for surface coating SSE such as $Na_{3.4}Zr_2Si_{2.4}P_{0.6}O_{12}$ for enhancing the electrochemical stability.[95] However, its binding abilities are not known despite being water-soluble. Hooper et al. reported an IC of 5×10^{-3} S cm^{-1} for Na_3PO_4 at 300 °C.[96]

Lithium dihydrogen phosphate (LHPO: LiH_2PO_4) is soluble in water and has also been reported to be a rather good ionic conductor. However, this conductivity is predominantly due to the conduction of protons (H^+) as confirmed by ^{1}H NMR investigations.[97] A recent study reported an IC of 2×10^{-5} S cm^{-1} at 200 °C and 1.6×10^{-8} S cm^{-1} at 60 °C, which was much lower than previously reported values.[43] This might be attributed to the fact that the LHPO pellet was first dried at 200 °C before recording the impedance. The IC of LPO ($LiPO_3$: obtained by dehydrating LHPO powder at 400 °C) was at least two orders of magnitude lower than that of LHPO.[43] The conduction mechanism of LHPO has been suggested to be interbond proton conduction coupled with the rotational motion of the PO_4 tetrahedral group.[98,99] The OH^- groups in LHPO could be helpful for suitable binding properties, which resulted in improved electrochemical performance as compared to LPO and PVdF.

The IC of sodium phosphates (STMP, SHMP, SPP) was also evaluated in a similar way. They exhibited an IC in the range from 10^{-6} Scm^{-1} at 200 °C to 10^{-10} S cm^{-1} at 60 °C (Figure 5b). The IC of amorphous STMP ($(NaPO_3)_3$) was one order of magnitude higher than the IC of the crystalline phase. This can be attributed to the change in their local structure. The amorphous phase has higher defect concentrations which facilitates ionic transport.

Sodium and lithium silicates have also been reported as ionic conductors. SMS (Na_2SiO_3) has been reported to possess a 3D Na^+ diffusion pathway.[70,71,100] Hydrated alkali silicates (water glasses) generally consist of mixtures of polymeric and oligomeric silicates and are largely protonated due to the weakness of silicic acid. Therefore, the influence of H^+ conductivity cannot be ruled out.[101] Molinelli et al.[102] found a mixed cation effect between Na^+ and H^+. They observed that water acts as a "pseudo alkali" at lower water concentrations by releasing H^+ in place of Na^+. The presence of H_2O in these systems provides greater free volume, rendering the alkali cation (Na^+) mobility more energetically favorable. Therefore the IC of SMS was recorded after heating it at 1000 °C to completely get rid of any residual water of crystallization and avoid an overestimation of its IC. The IC was observed to be in the range of other IABs (5.3×10^{-10} S cm^{-1} at 60 °C and 10^{-7} S cm^{-1} at 200 °C). Similar conductivities were observed for lithium polysilicate binder (LPS: $Li_2Si_5O_{11}$).[43] Due to pronounced scattering of the EIS data below 60 °C, the IC of IAB could not be estimated below 60 °C. The IC of lithium metasilicate (Li_2SiO_3) has been reported to be reasonably high (2.5×10^{-8} S cm^{-1} at 25 °C), but its poor water solubility restricts its usage as a binder.[103] However, it has been reported as a surface coating agent for several electrode materials.[104]

3. Solid-State Batteries

All-solid-state batteries (ASSBs) employing inorganic solid electrolytes have attracted tremendous interest in academia and industry in the past years due to their potentially high energy density.[105–107] These batteries use a solid pellet/disc of an electrolyte instead of a salt-solvent-based electrolyte and separator. Despite possessing interesting features and prospects, the large-scale commercialization of ASSBs has been challenging due to several obstacles. In fact, the SSEs need to provide high room temperature (RT) IC, mechanical stability, and interfacial stability along with sufficiently close contact with the electrode active materials—also when the latter change their volume upon (dis)charge.

Some advanced SSEs such as $Li_{10}GeP_2S_{12}$ (LGPS) provide now a very high IC of $\approx10^{-2}$ S cm^{-1}.[108] Nonetheless, the rate capability of most ASSBs employing high-voltage cathodes remains poor. This is mainly attributed to interfacial charge transport limitations between SSE and the electrode owing to a limited effective contact area, which is a crucial factor for electrochemical performance. This is further affected by potentially occurring reactions at the solid–solid interface. In the case of unstable interfaces, high resistances, and undesired side reactions are observed that adversely affect the rate capability in SSBs.[32,109,110] Ideally, any kind of interphase (formed in situ or applied artificially) is ideally a good ionic conductor but electronically insulating, as also summarized and highlighted in several excellent review articles on this subject.[105,111–115]

Generally, interfacial issues are broadly classified into physical and chemical aspects.[111] Poor ionic and electronic contact, dendrite growth, physical separation or mismatch, grain boundaries, volume changes, etc. are summarized under physical aspects. On the other hand, the formation of space charge layers, undesired reactions, and electrochemical instability are classified as chemical issues. It is commonly challenging to understand the detailed reasons behind high interfacial resistances and instability as it could be due to several reasons.

In addition to these factors, the usage of ionically insulating binders such as PVdF restricts the movement of ions in the bulk solid-state electrode in absence of liquid electrolyte (Figure 5a). In fact, even very small quantities of such binders (e.g., <3 wt%) contribute to considerably large internal resistances in ASSBs.[116–118] The usage of ionically conducting binder would provide a viable pathway to mitigate high interfacial resistances.

Several reports have claimed to employ ionically conducting binders for ASSB applications. For instance, a recent study by Hong et al.[119] reported an ionomer binder with reasonably high Li^+ conductivity (10^{-5} S cm^{-1}) in $LiNi_{0.7}Co_{0.1}Mn_{0.2}O_2$ cathodes (mass loading: 17 mg cm^{-2}) using a dry coating process on Li_6PS_5Cl (LPSCl) SSE. However, they also added 25 wt.% of SSE in the cathode. This combination achieved a stable

electrochemical performance (discharge capacity:180 mAh g^{-1} at 0.1C, 90% capacity retention after 300 cycles at 0.5C), but from a compositional perspective, 25 wt.% of SE in the cathode layer only added dead mass to the battery without any direct contribution to the capacity. In another study,[120] the authors fabricated ASSBs (Li//LPSCl//graphite-binder) using Li-CMC as binder without the use of any SSE or LE. Due to effective Li^+ conduction in Li-CMC, the internal resistance of the cell was reduced, and the final cell achieved higher areal and volumetric capacity as compared to Na-CMC and CMC-SBR comprising cells. The Li^+ and Na^+ conductivity in Li-CMC and Na-CMC, respectively were evaluated theoretically. The first principle calculations revealed that Li^+ interstitial formation energy in both Li-CMC and Na-CMC is at least 4.6 times lower than the Li/Na vacancy formation. This established that Li^+ interstitial migration is the dominant phenomenon for both Na-CMC and Li-CMC as potential alternative to IABs.

Binders with intrinsic IC and sufficient adhesion would be an ideal choice for ASSBs. Recently, we demonstrated a solid-state battery (SSB) using an IAB and also with organic binders such as PVdF, Na-CMC, and Na-PAA for comparison.[43] In the first approach (*Type-I SSB*), the cathode layer comprising P2-$Na_{0.7}Mn_{0.9}Mg_{0.1}O_2$ along with 10 wt.% conducting carbon and 10 wt.% PVdF binder was coated on one side of the sodium beta alumina SSE pellet (Figure 5c). The Na metal anode was pressed on the other side of the pellet. The cells showed negligible capacity due to high impedance (400 kΩ) at RT (Figure 5d). Similar trends were observed with other organic binders such as Na-CMC and Na-PAA. However, with the addition of a minuscule amount of LE on the cathode side (*Type-II SSB*), the impedance was reduced by several orders of magnitude and the cell could be operated smoothly (Figure 5d, inset). Although these cells functioned well, they were not true ASSBs as the ionic transport relied on the IC of the LE. When using an IAB instead (Type-III SSB), i.e., sodium phosphate (SHMP), as the binder, the cells showed an impedance of 80.5 kΩ at RT, which decreased to 6.8 kΩ at 80 °C (Figure 5e). The cells showed a discharge capacity of 100 mAh g^{-1} at 80 °C, which faded to 68 mAh g^{-1} after 10 cycles due to an increase in impedance during cycling (Figure 5f).

ASSB were also fabricated with organic binders such as Na-CMC and Na-PAA to verify the claims of their Na^+ conductivity. The cells showed negligible capacity along with high interfacial resistance similar to the PVdF-based cells owing to the poor Na^+ conductivity of such binders. These results proved that IAB hold the potential to improve the interfacial resistance in ASSBs. Their ion-conducting nature facilitates the transfer of Na^+ across the interfaces and in the electrode bulk, presumably via a "grain-boundary-type" charge transport. To further improve the cycling performance of ASSBs and to achieve greater RT stability, however, the IC of these IABs needs to be improved. Moreover, further optimization of, e.g., the electrode composition, fabrication, and an advanced interface engineering are needed to improve the electrochemical performance of IAB-based ASSBs.

4. Liquid-Electrolyte-Based Battery Cells

In this section, the electrochemical performance of anodes and cathodes in combination with IABs for lithium-ion and sodium-ion batteries comprising an LE is discussed.

4.1. Anodes

Carbon-based anodes are widely used in both lithium-ion and sodium-ion batteries, i.e., graphite in the case of LIBs and hard carbons in the case of SIBs.[121–124] In both cases, water-soluble and fluorine-free organic binders such as CMC, PAA, and alginate are commonly used.[31,35,37,125–127] Besides a substantially improved sustainability, the use of these binders resulted in an enhanced initial Coulombic efficiency, rate capability, and overall cycling performance.

Recently, Wei et al.[42] reported the use of IABs like LPS, LHPO, and SPP for graphite and silicon anodes for LIBs. The graphite slurry comprising IAB settled quickly and spread laterally on the copper foil. Also, the coatings with 10 wt.% of IAB showed poor adhesion with the current collector. To improve the coating quality, the authors attempted to use a very high and impractical binder content of 20 wt.%. The adhesion issue was mainly attributed to the poor bonding between graphite and the IAB due to a lack of surface functional groups in graphite. As an alternative, they recommended to use thickeners such as CMC to make the slurry more viscous. Very similar results were observed more recently in another study.[43] However, graphite-IAB slurries could be coated on a steel current collector due to the surface roughness of the steel (Figure 4a).[43] The electrodes delivered high capacities at low (dis)charge rates (up to 0.2C), but the capacity faded at a higher rate of 1C. To improve this, silicon oxide (SiO_x) was coated on graphite using a wet chemical synthesis (**Figure 6a**).[57] The silicon oxide polymorphs on coating acted as an intermediate layer between graphite and the IAB, which significantly improved the bonding between them. The coated graphite delivered a very stable cycling performance with silicate-based IAB such as LPS and SMS. A specific capacity of ≈315 mAh g^{-1} was achieved at 1C with a stable capacity retention for over 1000 cycles (Figure 6b). Even at high rates such as 20C, >90% capacity was retained after 4000 cycles in the case with SMS binder (Figure 6c). However, the silicon oxide-coated graphite was not very compatible with phosphate-based binders such as LHPO binders due to poor interaction between the silicon oxide coating and the phosphate groups of LHPO. Presumably, a phosphate-based coating such as Li_3PO_4 would be needed to achieve stable cycling with LHPO binder.

Promising results were also achieved for $Li_4Ti_5O_{12}$ (LTO) an alternative anode material. LTO was tested with two IABs (SHMP and LPO) along with PVdF.[43] Nevertheless, the LTO-IAB electrodes showed lower reversible capacities as compared to LTO-PVdF (Figure 6d). This was attributed to two main reasons, poor bonding between LTO and IAB and lithium leaching due to aqueous processing.

Some recent studies have also investigated IAB such as PTP, LPS, SPP, LHPO, and LMS for silicon anodes in LIB.[42,56,58] Despite many successful water-soluble binders for Si anodes, their poor dispersability on the Si active material cannot be neglected. Therefore, IABs with relatively smaller chain lengths have caught attention in addressing agglomerations issues. Feng et al.[58] studied PTP in combination with nanosized Si anodes for LIB. They achieved a charge capacity of 1739 mAh g^{-1} and a capacity retention of ≈99% after 80 cycles (Figure 6e). In comparison, CMC and PVdF comprising electrodes only retained 63% and 21%, respectively. During the long-term cycling, the Si-PTP

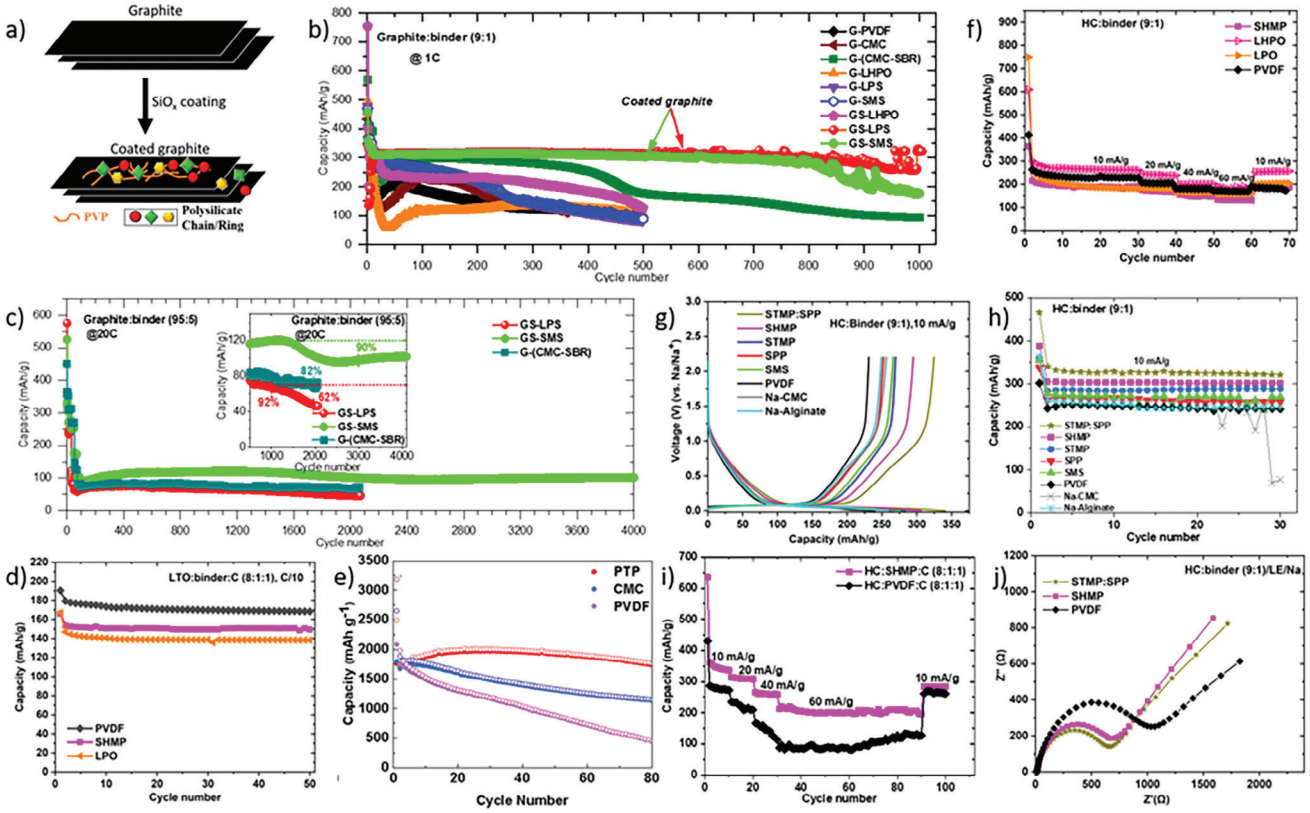

Figure 6. Electrochemical performance of graphite, $Li_4Ti_5O_{12}$ (LTO), silicon, and hard carbon (HC) anodes with inorganic aqueous binders (IAB) for LIBs and SIBs: a) Schematic of coated graphite. b) Cycling performance of graphite and silicon oxide coated graphite (GS) with different binders at 1C. c) Cycling performance of graphite (G) and silicon oxide coated graphite (GS) with different IABs at 20C. a–c) Reproduced with permission.[57] Copyright 2023, Elsevier. d) Cycling performance of LTO ($Li_4Ti_5O_{12}$) with different binders at 0.1C. e) Cycling performance of Si anode with different binders at a current density of 800 mA g^{-1}. Reproduced with permission[58] Copyright 2021, American Chemical Society. f) Rate capability test of hard carbon with different binders for LIB. g) Discharge–charge profile of hard carbon with different binders for SIB. h) Cycling performance of hard carbon with different binders at 10 mA g^{-1} for SIB. i) Rate capability of hard carbon along with conducting carbon and SHMP ($(NaPO_3)_6$) and PVdF binder. j) Impedance of HC:binder//liquid electrolyte//Na half-cell with PVdF, SHMP, and mixed binder. d,f–j) Reproduced with permission.[43] Copyright 2022, Royal Society of Chemistry.

electrodes achieved a capacity of 1280 mAh g^{-1} after 300 cycles at 800 mA g^{-1}, along with a capacity retention of 73%. The better performance of the Si-PTP electrodes was assigned to their superior mechanical properties such as better adhesion and higher Young's modulus in comparison with the organic binders. The better adhesion between Si and PTP due to abundant active sites (P═O, P—O^-, —OH) helped to withstand the extensive volume changes of the nanosized Si anode. In another report, Si-LMS electrodes provided an average discharge capacity of 663 mAh g^{-1} at 8.4 A g^{-1} after 100 cycles.[56] This superior performance was attributed to a favorable interface between LMS and the Si surface due to silicate-based adhesion and Li^+ transport channels within the binder. Notably, they also used citric acid to reduce the basicity of LMS, which was later removed by drying the electrodes at 300 °C.

IABs were also investigated as binders for hard carbon (HC) anodes for LIB and SIB. HC-LHPO electrodes outperformed other binders including PVdF for LIB (Figure 6f). For SIB, IAB-based hard carbon electrodes achieved high reversible capacities as compared to organic binders such as PVdF, Na-CMC, and Na-ALG. A mixed binder (MB: mixture of STMP and SPP) based hard carbon electrode delivered higher capacity as compared to the individual binders. These electrodes showed a reversible capacity of 340 mAh g^{-1} as compared to only 243 mAh g^{-1} for PVdF-containing electrodes at 10 mA g^{-1} (Figure 6g,h). All the IAB-based electrodes showed higher capacity as compared to organic binder (PVdF, CMC, ALG) based electrodes Adding conductive carbon improved the rate capability of the IAB-based electrodes. Also, the reversible capacity was improved by 17% to 360 mA h g^{-1} for the SHMP-based electrode (Figure 6i). This was attributed to enhanced ionic and electronic conductivity in hard carbon electrodes. In fact, the IAB-based cells showed lower impedance due to which the capacity of the plateau region of hard carbon could be modulated (Figure 6j). Lower overpotentials during discharge resulted in longer discharge plateaus of the hard carbon active material, which indicated a greater contribution of sodium storage in the nanopores of hard carbon. The electrochemical performance of carbon-based and silicon anodes has been summarized in **Table 2**.

Another report by Ransil and co-workers described sodium silicate ($Na_2O(SiO_2)_x$) as an inorganic adhesive capable of binding with diverse materials.[40] They demonstrated excellent cycling

Table 2. Electrochemical performance of carbon-based and silicon anodes. RC, reversible capacity; CR, capacity retention. *Pure silicon anode without conducting carbon was used.[42]

Binder	Graphite for LIB	Hard carbon for SIB	Hard carbon for LIB	Si anode for LIB
	Capacity at 1C, CR (No. of cycles), 10% binder, and 1-1.5 mg cm^{-2} of mass loading.	RC at 10 mAh g^{-1}, CR% (No. of cycles), 10% binder, and 2–3 mg cm^{-2} of mass loading	RC at 10 mA g^{-1}, CR (No. of cycles), 10% binder, and 2–3 mg cm^{-2} of mass loading	Capacity in mAh g^{-1}, CR% (No. of cycles), and mass loading (mg cm^{-2})
Organic binders	Pristine graphite, Ref. [57]	Ref. [43]	Ref. [43]	Ref. [42,56,58]
PVdF	158, 47% (400)	243, 60% (70) @10-60 mAg^{-1}; 85 $mAhg^{-1}$ @60 mAg^{-1} with additional 10% carbon.	264, 65% (70) @10-60 mAg^{-1}	• 31 (100), Ref. [56] • ≈0 mAh g^{-1} after first cycle, Ref. [42] • 449, 21% (80), Ref. [58]
CMC	160, 52% (≈400)	265, 95% (30) @10 mAg^{-1}	-	1139, 63% (80), Ref. [58], 0.5–0.7 mg cm^{-2}, 20% binder
Alginate	–	262, 94% (30), @10 mA g^{-1}	–	1860 (100), Ref. [56]
PAA	–	–	–	*1167, Ref. [42], 80.6% (100), 10% binder, 2 mg cm^{-2}
CMC-SBR	270, 92% (400), 64% (500)	–	–	–
Inorganic binders	SiO_x coated graphite, 10% binder, Ref. [57]	Ref. [43]	Ref. [43]	–
LPS	• 316, 95% (800) • 276 with 5% binder, 91% (1000)	–	214, 89% (70) @10–60 mA g^{-1}	*1122, Ref. [42], 71.5% (100), 10% binder, 2 mg cm^{-2}
SMS	311, 92% (800) 265 with 5% binder, 95% (1000)	276, 97% (30)@10 mAg^{-1}	–	–
LMS	-	-	-	2123 (100) at 0.84 A g^{-1} 663 at 8.4 Ag^{-1}, Ref. [56]
LHPO	Phosphate-based surface coating/ functionalization could be helpful.	–	301, 85% (70), @10-60 mAg^{-1}	*1032, Ref. [42] 82.5% (100), 10% binder, 2mgcm^{-2}
SHMP		306, 83% (70), @10-60 mAg^{-1}m; 220 $mAhg^{-1}$ @60 mAg^{-1} with additional 10% carbon.	215, 87% (70), @10-60 mAg^{-1}	–
STMP		283, 100% (30), @10 mAg^{-1}	–	–
SPP		262, 98% (30), @10 mAg^{-1}	–	*1128, Ref. [42] 81% (100), 10% binder, 2 mg cm^{-2}
PTP		-	–	1739 @ 800 mA g^{-1}, 99% (80) 1279 @ 800 mA g^{-1}, 72.7% (300) 0.5–0.7 mg cm^{-2}, 20% binder, Ref. [58]

stability of $LiFePO_4$ and graphite electrodes with sodium silicate as the binder. The authors also showcased the electrochemical performance of a structural battery that was fabricated by producing robust and free-standing composite electrodes, exploiting the suitable ionic transport properties and high thermal stability of this binder. The resulting structural battery exhibited a specific energy of 93.9 Wh kg^{-1} along with a high tensile modulus of 1.4 GPa.

4.2. Cathodes

The aqueous processing of oxide-type cathode materials is still a challenge owing to their high reactivity with water.[35,128,129] For instance, when lithium or sodium transition metal oxides are exposed to water, it results in the formation of carbonate and hydroxide species, lithium or sodium leaching, and a very basic slurry with a pH higher than 8. This causes the aluminum current collector to corrode, which eventually causes cracks and voids in the dry electrodes.[130–133] Additionally, proton exchange with cathode materials results in capacity loss and adverse reactions.[35,128,129]

We recently investigated the potential of IABs to overcome the limitations of conventional organic aqueous binders. The electrodes made of these binders exhibited excellent electrochemical performance. When tested with a $Na_{0.7}Mn_{0.9}Mg_{0.1}O_2$ (NMO) cathode active material, the SHMP binder-based electrodes showed 28% higher capacity retention after 150 cycles as compared to the PVdF-based electrode (**Figure 7**a,b). With the $Na_3V_2(PO_4)_3$ (NVP) cathode (Figure 7c,d), all electrodes retained 94% of their capacity after 150 cycles. However, at all rates studied, the NVP-STMP and NVP-MB electrodes completely outperformed PVdF-based electrodes.[43] In another study, P2-$Na_{0.67}Mn_{0.67}Ni_{0.33}O_2$ (NMNO) electrodes with an STMP binder have been reported to exhibit a high capacity retention of 65% after 200 cycles, which was higher than electrodes based on CMC (61%) and PVdF (21%) (Figure 7e,f).[134] The electrochemical performance is summarized in **Table 3**.

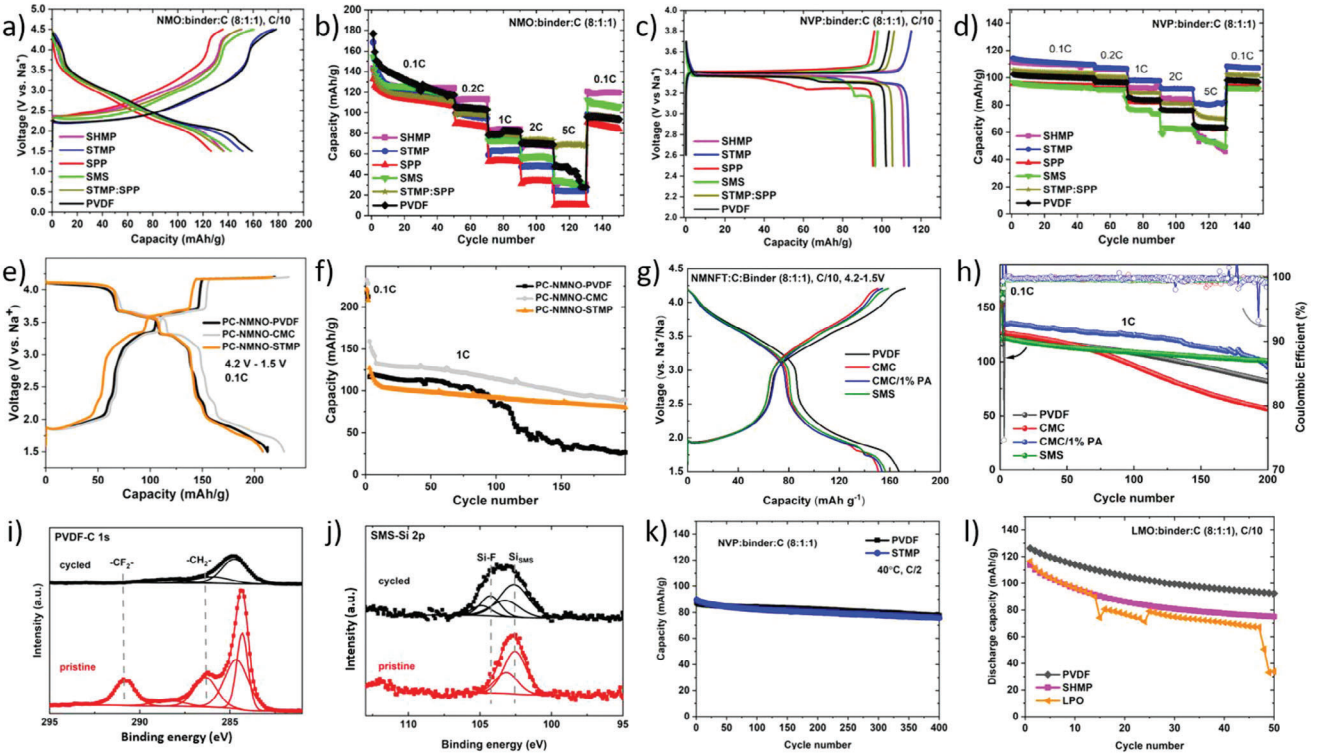

Figure 7. Electrochemical performance and characterization of different cathode materials with inorganic aqueous binders (IAB) and organic binders for SIB and LIB. a) Second charge–discharge profile of $Na_{0.7}Mn_{0.9}Mg_{0.1}O_2$ (NMO)cathodes. b) Corresponding rate capability of NMO cathode. c) Second charge-discharge profile of $Na_3V_2(PO_4)_3$ (NVP) cathode. d) Corresponding rate capability of NVP cathode. a–d) Reproduced with permission.[43] Copyright 2022, Royal Society of Chemistry. e) Second charge–discharge profile of $Na_{0.67}Mn_{0.67}Ni_{0.33}O_2$ (NMNO) cathode. f) Corresponding cycling performance of NMNO cathode. e,f) Reproduced with permission.[134] (under review). g) Second charge–discharge profile of $Na_{0.67}Mn_{0.55}Ni_{0.25}Fe_{0.1}Ti_{0.1}O_2$ (NMFT) cathode. h) Corresponding cycling performance of NMFT cathode. i) XPS of pristine and cycled electrodes of NMFT-PVdF. j) XPS of pristine and cycled electrodes of NMFT-SMS. g–j) Reproduced with permission.[45] (under review). k) Cycling performance of NVP with PVdF and STMP ($(NaPO_3)_3$) binders at 40 °C. l) Cycling performance of $LiMn_2O_4$ (LMO) cathode with SHMP ($(NaPO_3)_6$), LPO ($LiPO_3$), and PVdF binders for LIB. k,l) Reproduced with permission.[43] Copyright 2022, Royal Society of Chemistry.

In another recent report, multifunctionalities of SMS binder with P2-$Na_{0.67}Mn_{0.55}Ni_{0.25}Fe_{0.1}Ti_{0.1}O_2$ (NMNFT) were investigated (Figure 7g,h).[45] There were no discernible differences observed in the charge-discharge profiles of the aqueous binder-based electrodes compared to the PVdF, except that all aqueous binder electrodes exhibited slightly lower reversible capacities compared to the PVdF-based electrodes. This was attributed to the loss of Na^+ and/or the Na^+/H^+ exchange during aqueous processing. The NMNFT-SMS electrodes delivered a reversible capacity of 161 mAh g^{-1} and retained 83% of the initial capacity after 200 cycles at a rate of 1 C, whereas the PVdF and CMC-based electrodes retained only 66% and 55%, respectively (Figure 7h). Furthermore, decreased cell impedance and faster Na^+ diffusion have been reported for the NMNFT-SMS electrodes, resulting in better rate performance. XPS (Figure 7i,j) and TEM analysis confirmed that the SMS binder created a homogeneous and stable nanoscale layer over the cathode particle surface, protecting the particle from exfoliation/cracking caused by electrolyte attack and/or volume variations caused by repetitive charge–discharge cycling. Because of its great binding ability and surface coverage, such passivating layers also aid cathode materials in avoiding transition metal dissolution/degradation, which further helped in suppressing/delaying the P2′ phase transition during cycling as confirmed by the *operando* XRD study. High temperature (40 °C) measurements with NVP-IAB maintained a stable capacity of 80 mAh g^{-1} even after 400 cycles at C/2 (Figure 7k).[43] $LiMn_2O_4$ (LMO) cathode was also tested against SHMP and LPO binders and compared with PVdF for LIB. All these systems showed capacity fading possibly due to Li^+ exchange during aqueous processing.

Overall, the improved electrochemical performance of IABs is attributed to their high binding strength, uniform distribution/coverage of the binder on the active material/carbon particles, and improved kinetics due to their intrinsic IC. To further improve their performance and deter the leaching of metal ions during aqueous processing, suitable surface coatings and single crystalline cathode morphology could be helpful.

4.3. Surface Coatings

Due to relatively large surface tension (water: 72.8 mN m^{-1}, NMP: 40.8 mN m^{-1} at 20 °C), water-based slurries are difficult to coat on the current collector such as aluminum or copper foil.[135–137] It is therefore much easier for the electrode to be detached causing decay in the capacity. Apart from this, electrode materials

Table 3. Comparison of the electrochemical performance of different cathode materials with different aqueous binders.

Cathode	Binder	Reversible capacity [mAh g^{-1}], voltage window	Capacity retention (cycles) @ C-rate	Reference
P2-$Na_{0.7}Mn_{0.9}Mg_{0.1}O_2$ (NMO), Mass loading: 2–3 mg cm^{-2}	NMO: C: binder (8:1:1)	@0.1C, 4.5-1.5 V	0.1–5C (150 cycles)	[43]
	SHMP	137	87%	
	STMP	152	61%	
	SPP	126	66%	
	SMS	142	74%	
	Mixed binder, STMP: SPP (1:1)	136	69%	
	PVdF	159	59%	
$Na_{0.67}Mn_{0.67}Ni_{0.33}O_2$ (NMNO), Mass loading: ≈5 mg cm^{-2}	NMNO: C: binder (8:1:1)	@0.1C, 4.2-1.5 V	-	Under review[134]
	STMP	208	65% (200)	
	PVdF	212	27% (175) @1C	
			21% (200)	
	CMC	228	61% (200)	
$Na_{0.67}Mn_{0.55}Ni_{0.25}Fe_{0.1}Ti_{0.1}O_2$	NMFT:C:binder (8:1:1)	@0.1C, 4.2–1.5 V	-	Under review[45]
	SMS	162	87% (100) @0.2C	
(NMNFT), Mass loading: ≈4 mg cm^{-2}			83% (200) @1C	
	PVdF	168	80% (100) @0.2C	
			66% (200) @ 1C	
	CMC	152	89%(100) @ 0.2C	
			56% (200) @ 1C	
	CMC/1% PA	159	88% (100) @ 0.2C	
			81% (175)@1C	
$LiFePO_4$ (LFP)	SMS, 1.6 mg cm^{-2}	≈90 @1C, stable for >700 cycles. Better performance as compared to PVDF at higher mass loading.	Energy density of 93.9 Wh kg^{-1} in structural battery at 0.2C	[40]

particularly cathodes in SIBs and LIBs suffer from several other challenges such as high-temperature and/or high-voltage capacity fading, triggered by unfavorable side reactions. Apart from this, issues such as transition metal dissolution lead to the deterioration of the cathode structure. To counter these challenges, the application of suitable surface coatings appears as a suitable approach, as it allows to stabilize and reduce undesired reactions.[138,139] Out of the numerous surface coating materials investigated to date, Na and Li phosphates and silicates will be discussed here; i.e., those materials that have also been investigated as IABs already.

4.3.1. Phosphate-Based Coatings

Phosphates in general have optimum ionic conductivity as well as thermal stability.[138,140] Sodium and lithium phosphates have been utilized for coating various electrode materials with the aim of improving their electrochemical and thermal properties. They are of interest also due to their low cost and easy processability. Metal phosphate-based coatings barely diffuse into the bulk, even if sintered at high temperatures due to the strong bonding energy of the PO_4^{3-} anion.[141] In this regard, several metal phosphate coatings such as $AlPO_4$, $Co_3(PO_4)_2$, $Ni_3(PO_4)_2$, and $FePO_4$ have been employed with various cathodes in SIBs and LIBs.[138,142]

$NaPO_3$ coatings on cathode materials have been reported to perform multiple functions such as facilitating ionic transport and scavenging HF and H_2O from the electrolyte, thus avoiding HF attack.[138] It has been investigated with manganese-based sodium layered oxides as a surface coating agent for improved electrochemical performance. Jo et al.[70] for instance coated 10 nm thin layers of $NaPO_3$ on P2-type $Na_{2/3}(Na_{1/3}Mn_{2/3})O_2$ via the melt impregnation method by mixing the active material with ammonium phosphate ($NH_4H_2PO_4$) followed by a heat treatment at 300 °C (**Figure 8a**). The sodium residues at the surface react with ammonium phosphate to form a thin $NaPO_3$ layer (Figure 8b). This $NaPO_3$-coated cathode exhibited significantly improved electrochemical performance due to the suppression of undesired side reactions arising from the decomposition of the electrolytic salt, which was confirmed by various characterization techniques (Figure 8c). The $NaPO_3$ layers scavenged HF and H_2O from the electrolyte and delayed the decomposition to Mn_3O_4, thereby suppressing oxygen release in the highly desodiated state. In another report by Li et al.,[143] $NaPO_3$ coating on P2-$Na_{0.7}MnO_{2.05}$ was carried out via a similar approach. The coated cathode showed superior rate capability and cycling performance for both solid-state and LE-comprising battery cells. These coatings have also been explored for O3-type sodium layered oxides via a solution-based method.[144] 1 wt.% of the coating showed improved cycle life and improved air stability. Higher coating

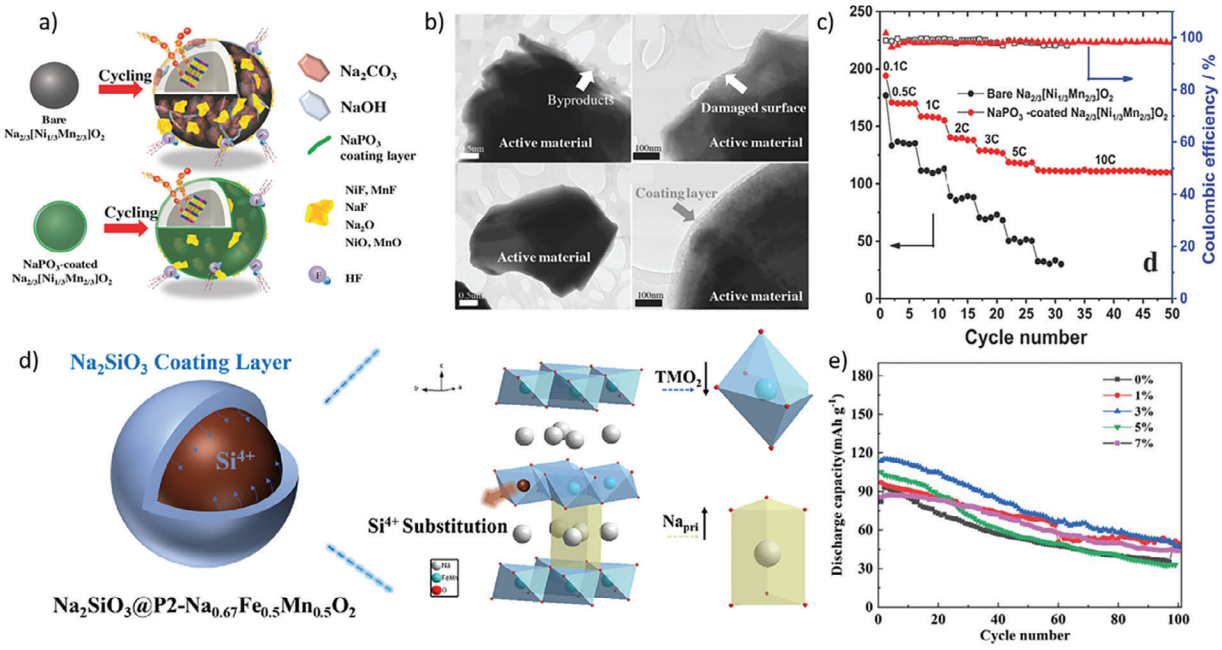

Figure 8. Surface coating: a) Schematic representation of by-products on the surface of bare and $NaPO_3$ coated $Na_{2/3}(Na_{1/3}Mn_{2/3})O_2$. b) Low and high magnification TEM images of $NaPO_3$ coated and uncoated $Na_{2/3}(Na_{1/3}Mn_{2/3})O_2$ cathode after cycling. c) Rate capability of coated and bare samples. a–c) Reproduced with permission.[70] Copyright 2018, Wiley-VCH. d) Schematic of Na_2SiO_3 (SMS) coated $Na_{0.67}Fe_{0.5}Mn_{0.5}O_2$ (NFMO) cathode. e) Cycling performance of pristine and SMS-coated NFMO cathode. e,f) Reproduced with permission.[71] Copyright, 2021, Elsevier.

concentrations led to sodium leaching from the bulk, resulting in the formation of metal oxides and metal phosphates (reaction of TM with phosphate groups), thereby increasing the polarization and reducing the reversible capacity.

Similarly, lithium phosphate coatings have been applied to LIB cathodes to pursue an improvement in electrochemical performance. Li_3PO_4 surface coatings have been applied to almost all classes of LIB cathodes due to their ionically conducting, chemically and electrochemically inert, and thermally stable nature. Tang et al.[141] realized a Li_3PO_4 coating on $LiNi_{0.815}Co_{0.15}Al_{0.035}O_2$ (NCA) material by coating ammonium phosphate on the surface of the hydroxide precursor before mixing it with Li_2CO_3, followed by a sintering step at 750 °C. The ammonium phosphate also helped to remove the lithium residues (LiOH, Li_2CO_3) from the NCA surface. An improved electrochemical performance was achieved for samples with reasonably thick coatings at RT and 55 °C. The coated samples also exhibited 30% less heat evolution as compared to the bare sample. Another report by Su et al.[145] presented uniformly coated Li_3PO_4 on the surface of $Li_{1.2}Ni_{0.2}Mn_{0.6}O_2$ cathode using a wet chemical method. The cycling stability of the coated sample was improved from 65% to 76% after 100 cycles. Disordered Li_3PO_4 films on $LiCoO_2$ increased the power density by 50% by reducing the polarization at the interface.[146] Similarly, Li_3PO_4 coatings have been investigated on several other cathode materials.[147–150]

4.3.2. Silicate-Based Coatings

Silicates of lithium and sodium have been proven to be promising surface coating materials due to their ionically conducting nature, low cost, easy processability, and structural stability in organic electrolytes. Lithium silicates have also been applied as solid-state electrolytes.[151] Jiao et al.[71] utilized a collaborative strategy of doping and surface coating to improve the electrochemical performance of layered oxide cathodes (Figure 8d,e). The phase transitions (P2-OP4) in P2-type layered oxides are accompanied by a large lattice volume change along with the change of the lattice in the c direction. To address these issues, they coated P2-$Na_{0.67}Fe_{0.5}Mn_{0.5}O_2$ with sodium metasilicate (SMS: Na_2SiO_3). The cathode particles and tetraethyl orthosilicate (TEOS: $Si(OC_2H_5)_4$) were dispersed in deionized water followed by a sintering step that resulted in the in-situ formation of Na_2SiO_3 on the cathode surface. During the stirring step, TEOS undergoes hydrolysis to form SiO_2 that further reacts with surface impurities such as Na_2CO_3 to form SMS during sintering. The shift of (002) peak shift of 3 wt.% coated sample toward the lower angle confirmed an increase of interlayer spacing due to the migration and doping with Si^{4+}. The synergetic effect of coating and doping showed improved rate capability and cycling performance due to enlarged interlayer spacing caused by Si^{4+} doping, avoiding unwanted side reactions and providing 3D diffusion channels provided by SMS coating. Compared to the bare sample (10^{-14} cm^2s^{-1}), the 3 wt.% coated sample (10^{-13} cm^2 s^{-1}) showed a one order of magnitude higher diffusion coefficient, thereby supporting the efficient intercalation and deintercalation of Na^+. Lithium silicate (Li_4SiO_4, $Li_2Si_2O_5$) coatings have been studied with cathode materials such as olivine $LiFePO_4$ and spinel $LiNi_{0.5}Mn_{1.5}O_4$ cathode materials.[152–154] Yang and coworkers synthesized lithium silicate coatings on $LiNi_{0.5}Mn_{1.5}O_4$ using SMS (Na_2SiO_3) as a silica precursor.[153] SMS is hydrolyzed to form small-sized $H_2SiO_4^{4-}$ and $H_3SiO_4^-$ micelles anchored

on the surface of the cathode particles. These micelles undergo a condensation reaction and form an SiO_2 layer at a favourable pH value of 10. These coatings were helpful in reducing side reactions and facilitating the charge transfer, leading to higher capacity and cycling stability as compared to the pristine samples at RT and 55 °C.

5. Environmental Profile and Economic Implications of Binders

Sustainability assessments have become a common approach to support technology development and decision-making processes. Different tools and methods are available for the evaluation of the potential effects of a system on the environment and society.[155,156] Concerns associated with battery systems such as resource criticality, safety issues, and toxicity can thus be addressed via some of these methodologies.[157,158] Several life cycle assessments (LCAs)[159,160] and toxicity analysis[161,162] of the battery production process can be found in the literature but, to the best of our knowledge—no detailed sustainability analysis of IAB has been conducted so far. Within these LCAs, the environmental impacts of a battery system are typically quantified based on 1 kWh of storage capacity. These impacts are associated with the material and energy flows necessary to manufacture a system capable of delivering this capacity. At the same time, battery capacity and mass composition are interrelated via performance parameters such as energy density, cycle life, and charge/discharge efficiency. Because of the great influence of these parameters on the environmental profile of the battery, detailed analysis is required to bring into consideration potential changes in technical performance that may arise when substituting material or components such as binders. First observations already suggest that the substitution of conventional binders (e.g., PVdF) with IAB could potentially lead to improvements in performance,[43] which may also improve the environmental profile of such batteries.

Although PVdF can be considered relatively safe for use in many applications, its use in batteries for electrode slurry preparation is conditioned by the additional need for NMP as a solvent. According to the regulation of the European Parliament on classification, labeling, and packaging,[163] the European Chemicals Agency—ECHA has classified NMP (CAS number 872-50-4) as a reproductive toxicant, which may also cause serious skin and eye irritation and damage to the nervous system among other effects.[164] For this reason, in addition to its high cost, NMP is usually recovered and reused in battery production. The water-soluble styrene-butadiene rubber (SBR, CAS number 9003-55-8), another commonly used binder, has also been classified as carcinogenic with the potential to cause germ cell. No hazard statements have been reported for CMC (CAS number 9000-11-7), which is another frequently used water-soluble binder. Among the inorganic binders, sodium metasilicate (SMS) is reported as potentially hazardous to human health, could cause skin corrosion and serious eye damage after exposure and, because of its capacity to make water acidic, it may pose a hazard to aquatic environments.

Recovery rates of about 99% for NMP reuse in new slurries have been reported, which prevents further exposure to the biosphere. However, to do so, additional measures such as condensation units and exhaust air treatment systems need to be implemented to collect and recycle the solvent. Additionally, small amounts of NMP may still be released into the atmosphere and the recovery rates can vary according to the production plant size. Lower recovery rates would lead to higher environmental impacts from solvent production and atmospheric exposure. This may accentuate the benefits of using water-soluble IABs in smaller production plants, as water is more readily available and can be freely released into the atmosphere. In fact, it has been found that a twofold reduction in electrode processing costs (which account for 8–9% of total pack cost), can be expected when using water-soluble binders instead of PVdF and associated NMP.[165] These cost reductions stem mainly from a simpler drying process and the avoidance of a solvent recovery unit, which also decreases energy demand. Additionally, the authors estimate up to $3–6 M savings in associated plant equipment for a plant producing ≈100 000, 10 kWh packs per year.

It can be expected that a decrease in energy demand during electrode production, produced by the use of water as solvent instead, will consequently lead to a decrease in the carbon footprint of the battery as well as to a decrease in other emissions associated to power generation (which vary according to the electricity mix being used). The potential impacts from direct emissions of supply chain and synthesis of IABs need still to be studied in detail. However, it is worth noting that the synthesis of several Na-based IABs involves sodium phosphate as a precursor,[166,167] which at the same time demands for phosphoric acid. The supply chain of phosphoric acid is associated to a release of hexavalent chromium (Chromium VI) into the biosphere (as found in Ecoinvent 3.8 database (ecoivent.org)), which has been reported by the US Environmental Protection Agency (EPA) as a genotoxic carcinogen. This may translate into a high human toxicity potential for these binders. Other potential effects of PVdF substitution, for instance at the End-of-Life of the battery need yet to be assessed. In particular, there are concerns and ongoing research regarding the toxicity and potentially adverse effects of fluoropolymers (PFAS) on humans and the environment, especially uncertain during the final disposal and end of their life cycle.[168] Given their persistence in the environment and the likelihood of human exposure, benefits could be expected from a substitution with IABs.

6. Conclusions and Outlook

The aqueous processing of battery electrodes is an essential step toward sustainable battery production. IABs as a rather recent class of binding agents are a potential alternative to common organic aqueous binders owing to their peculiar characteristics such as higher thermal stability, increased ionic conductivity, and potentially easier recycling. Relatively well-investigated classes of IABs are lithium and sodium phosphates and silicates. In addition to the aforementioned advantages, these binders are commonly composed of widely available elements and exhibit high adhesion strength for a wide range of electrode materials for SIBs and LIBs. The adhesion—and thus the electrochemical performance of the electrode—can be further improved by functionalizing the surface of the electrode material, yielding a stronger interaction between the active material and the IAB. Silicate and phosphate-based surface coatings, for instance, appear beneficial when employing silicate and phosphate-based binders

respectively. Their ionically conducting nature could be specifically beneficial for ASSBs and the realization of thicker electrodes. Nevertheless, it needs to be further improved for operating the ASSBs at ambient temperatures, which requires an in-depth understanding of the charge transport processes in such composites. This is generally also true for the detailed binding mechanism. In fact, the frequently rigid nature of such binders might benefit from hybridizing or smartly combining them with a minor fraction of a very elastic (thermally still very stable) organic phase to fine-tune the mechanical and electrochemical properties for a given application.

In fact, given the relatively early development stage of such binders, there is still plenty of room to explore their complete potential. Moreover, the utilization of IABs is not limited to SIBs and LIBs but can also be extended to other battery systems such as potassium-ion or magnesium-ion batteries by utilizing their water-soluble alkali salts, rendering this research field of great interest for the development of high-performance next-generation batteries.

Acknowledgements

The support of German Research Foundation (DFG) under project ID 390874152 (POLiS Cluster of Excellence, EXC 2154) is greatly acknowledged. P.B. thanks the Alexander von Humboldt Foundation (Bonn, Germany) for a 2022 Humboldt fellowship for experienced researchers. The help of Mr. Christian Grupe (KIT) in designing the schematics is gratefully acknowledged.

Open access funding enabled and organized by Projekt DEAL.

Author Contributions

S.T.: Sections 1–3, 4.1, 4.3, and Figures 1–6 and 8; V.P.: section 4.2 and Figure 7. S.P.B., F.A.S., and M.W.: Section 5; S.T. and D.B.: Section 6; all the authors discussed and planned the draft. M.W., P.B., D.B., and M.F. edited and revised te final manuscript.

Keywords

aqueous binders, inorganic binders, lithium-ion batteries, sodium-ion batteries, surface coatings

Received: October 4, 2023
Revised: November 14, 2023
Published online:

[1] M. Li, J. Lu, Z. Chen, K. Amine, *Adv. Mater.* **2018**, 30.
[2] P. K. Nayak, L. Yang, W. Brehm, P. Adelhelm, *Angew. Chem., Int. Ed.* **2018**, *57*, 102.
[3] J.-M. Tarascon, *Joule* **2020**, *4*, 1616.
[4] C. Delmas, *Adv. Energy Mater.* **2018**, *8*, 201703137.
[5] A. M. Skundin, T. L. Kulova, A. B. Yaroslavtsev, *Russ. J. Electrochem.* **2018**, *54*, 113.
[6] H. Hou, X. Qiu, W. Wei, Y. Zhang, X. Ji, *Adv. Energy Mater.* **2017**, *7*, 1602898.
[7] T. Perveen, M. Siddiq, N. Shahzad, R. Ihsan, A. Ahmad, M. I. Shahzad, *Renew. Sust. Energ. Rev.* **2020**, *119*, 109549.
[8] W. Zhang, F. Zhang, F. Ming, H. N. Alshareef, *EnergyChem* **2019**, *1*, 100012.
[9] M. Lao, Y. Zhang, W. Luo, Q. Yan, W. Sun, S. X. Dou, *Adv. Mater.* **2017**, *29*, 201700622.
[10] Q. Liu, Z. Hu, W. Li, C. Zou, H. Jin, S. Wang, S. Chou, S.-X. Dou, *Energy Environ. Sci.* **2021**, *14*, 158.
[11] C. Shi, L. Wang, X.' Chen, J. Li, S. Wang, J. Wang, H. Jin, *Nanoscale Horiz.* **2022**, *7*, 338.
[12] T. Jin, H. Li, K. Zhu, P.-F. Wang, P. Liu, L. Jiao, *Chem. Soc. Rev.* **2020**, *49*, 2342.
[13] X. Xiang, K. Zhang, J. Chen, *Adv. Mater.* **2015**, *27*, 5343.
[14] K. Westman, R. Dugas, P. Jankowski, W. Wieczorek, G. Gachot, M. Morcrette, E. Irisarri, A. Ponrouch, M. R. Palacín, J.-M. Tarascon, P. Johansson, *ACS Appl. Energy Mater.* **2018**, *1*, 2671.
[15] F. Gebert, J. Knott, R. Gorkin, S.-L. Chou, S.-X. Dou, *Energy Storage Mater.* **2021**, *36*, 10.
[16] A. Ponrouch, D. Monti, A. Boschin, B. Steen, P. Johansson, M. R. Palacín, *J. Mater. Chem. A* **2015**, *3*, 22.
[17] Z. Lin, Q. Xia, W. Wang, W. Li, S. Chou, *InfoMat* **2019**, *1*, 376.
[18] C. Bommier, X. Ji, *Small* **2018**, *14*, 1703576.
[19] Z. Zhang, T. Zeng, Y. Lai, M. Jia, J. Li, *J. Power Sources* **2014**, *247*, 1.
[20] Y. Lee, *Energies* **2019**, *12*, 658.
[21] H.-K. Park, B.-S. Kong, E.-S. Oh, *Electrochem. Commun.* **2011**, *13*, 1051.
[22] L. Han, T. Liu, O. Sheng, Y. Liu, Y. Wang, J. Nai, L. Zhang, X. Tao, *ACS Appl. Mater. Interfaces* **2021**, *13*, 45139.
[23] J. Xu, S.-L. Chou, Q.-F. Gu, H.-K. Liu, S.-X. Dou, *J. Power Sources* **2013**, *225*, 172.
[24] J. E. Marshall, A. Zhenova, S. Roberts, T. Petchey, P. Zhu, C. E. J. Dancer, C. R. McElroy, E. Kendrick, V. Goodship, *Polymers* **2021**, *13*, 1354.
[25] M. Zheng, X. Fu, Y. Wang, J. Reeve, L. Scudiero, W.-H. Zhong, *ChemElectroChem* **2018**, *5*, 2288.
[26] J. Qian, C. G. Wiener, Y. Zhu, B. D. Vogt, *Polymer* **2018**, *143*, 237.
[27] S. Li, Z. Xiao, K. Guo, H. Gan, J. Wang, Y. Zhang, L. Yu, Z. Xue, *Langmuir* **2020**, *36*, 9616.
[28] S. S. Zhang, T. R. Jow, *J. Power Sources* **2002**, *109*, 422.
[29] B. Jin, Y. Li, J. Qian, X. Zhan, Q. Zhang, *ChemElectroChem* **2020**, *7*, 4158.
[30] S. S. Sharma, A. Manthiram, *Energy Environ. Sci* **2020**, *13*, 4087.
[31] D. Bresser, D. Buchholz, A. Moretti, A. Varzi, S. Passerini, *Energy Environ. Sci.* **2018**, *11*, 3096.
[32] W. D. Richards, L. J. Miara, Y. Wang, J. C. Kim, G. Ceder, *Chem. Mater.* **2016**, *28*, 266.
[33] X. Han, Y. Gong, K. (K.) Fu, X. He, G. T. Hitz, J. Dai, A. Pearse, B. Liu, H. Wang, G. Rubloff, Y. Mo, V. Thangadurai, E. D. Wachsman, L. Hu, *Nat. Mater.* **2017**, *16*, 572.
[34] N. Lingappan, L. Kong, M. Pecht, *Renewable Sustainable Energy Rev.* **2021**, *147*, 111227.
[35] R.-R. Li, Z. Yang, X.-X. He, X.-H. Liu, H. Zhang, Y. Gao, Y. Qiao, L. Li, S.-L. Chou, *Chem. Comm.* **2021**, *57*, 12406.
[36] H. Chen, M. Ling, L. Hencz, H. Y. Ling, G. Li, Z. Lin, G. Liu, S. Zhang, *Chem. Rev.* **2018**, 118.
[37] T. C. Nirmale, B. B. Kale, A. J. Varma, *Int. J. Biol. Macromol.* **2017**, *103*, 1032.
[38] S.-L. Chou, Y. Pan, J.-Z. Wang, H.-K. Liu, S.-X. Dou, *Phys. Chem. Chem. Phys.* **2014**, *16*, 20347.
[39] A. M. Pillai, P. S. Salini, B. John, M. T. Devassy, *Energ. Fuel.* **2022**, *36*, 5063.
[40] A. Ransil, A. M. Belcher, *Nat. Commun.* **2021**, *12*, 6494.
[41] A. Kay, US20110117432A1, **2011**.
[42] C. Wei, M. N. Obrovac, *J. Electrochem. Soc.* **2021**, *168*, 020505.
[43] S. Trivedi, V. Pamidi, M. Fichtner, M. Anji Reddy, *Green Chem.* **2022**, *24*, 5620.

[44] G. Zhou, K. Liu, Y. Fan, M. Yuan, B. Liu, W. Liu, F. Shi, Y. Liu, W. Chen, J. Lopez, D. Zhuo, J. Zhao, Y. Tsao, X. Huang, Q. Zhang, Y. Cui, *ACS Cent. Sci.* **2018**, *4*, 260.
[45] R. Xu, V. Pamidi, Y. Tang, S. Fuchs, H. Stein, B. Dasari, Z. Zhao-Karger, S. Behara, Y. Hu, S. Trivedi, A. R. Munnangi, P. Barpanada, M. Fichtner, Greener, Safer and Better Performing Aqueous Binder for Positive Electrode Manufacturing of Sodium Ion Batteries (under review).
[46] O. M. Gutiérrez, *Adv. Chronic Kidney Dis.* **2013**, *20*, 150.
[47] L. E. Lampila, *Ann N Y Acad. Sci.* **2013**, *1301*, 37.
[48] E. J. Lowe, W. D. Adair, E. Johnston, *J. Am. Oil Chem. Soc.* **1978**, *55*, 32.
[49] Y. A. Owusu, *Adv. Colloid Interface Sci.* **1982**, *18*, 57.
[50] I. Izdebska-Szanda, A. Balinski, *Procedia Eng* **2011**, *10*, 887.
[51] S. Dieter, F. Werner, *Paints, Coatings and Solvents*, Wiley, Hoboken, NJ **1998**.
[52] Z. Zhang, H. Chen, Y. Wang, G. Wang, L. Li, M. Zhong, H. Bai, *Surf. Coat. Technol.* **2022**, *448*, 128868.
[53] G. Gettwert, W. Rieber, J. Bonarius, *J. Bonarius, Surf. Coat. Int.* **1998**, *81*, 596.
[54] S. Gupta, Y. M. Puttaiahgowda, A. Nagaraja, M. D. Jalageri, *Polym. Adv. Technol.* **2021**, *32*, 4642.
[55] D. G. Fauteux, J. Shi, US5856045A **1999**.
[56] X. Wang, K. Wang, Z. Zheng, Z. Wan, J. Zhao, H. Li, W. Jiang, Z. Wu, B. Chen, Y. Tan, M. Ling, M. Sun, C. Liang, *J. Colloid Interface Sci.* **2023**, *652*, 971.
[57] S. Trivedi, S. Dinda, Y. Tang, S. Fuchs, V. Pamidi, H. S. Stein, A. R. Munnangi, M. Fichtner, *J. Energy Storage* **2023**, *73*, 109210.
[58] J. Feng, D. Wang, Q. Zhang, J. Liu, Y. Wu, L. Wang, *ACS Appl. Mater. Interfaces* **2021**, *13*, 44312.
[59] H. M. Ondik, *Acta. Crystallogr.* **1965**, *18*, 226.
[60] T. Glonek, *Origins Life Evol. Biospheres* **2021**, *51*, 1.
[61] P. Richet, B. O. Mysen, D. Andrault, *Phys. Chem. Miner.* **1996**, *23*, 157.
[62] A. Grund, M. Pizy, *Acta Crystallogr.* **1952**, *5*, 837.
[63] R. Zosiamliana, Lalrinkima, B. C., G. Abdurakhmanov, M. P. Ghimire, D. P. Rai, *RSC Adv.* **2022**, *12*, 12453.
[64] M. N. Richard, J. R. Dahn, *J. Electrochem. Soc.* **1999**, *146*, 2078.
[65] H. Maleki, G. Deng, I. Kerzhner-Haller, A. Anani, J. N. Howard, *J. Electrochem. Soc.* **2000**, *147*, 2930.
[66] A. Kriston, I. Adanouj, V. Ruiz, A. Pfrang, *J. Power Sources* **2019**, *435*, 226774.
[67] S. Ma, M. Jiang, P. Tao, C. Song, J. Wu, J. Wang, T. Deng, W. Shang, *Prog. Nat. Sci.: Mater. Int.* **2018**, *28*, 653.
[68] J.-I. Yamaki, Y. Baba, N. Katayama, H. Takatsuji, M. Egashira, S. Okada, *J. Power Sources* **2003**, *119–121*, 789.
[69] T. Yoon, S. Park, J. Mun, J. H. Ryu, W. Choi, Y.-S. Kang, J.-H. Park, S. M. Oh, *J. Power Sources* **2012**, *215*, 312.
[70] J. H. Jo, J. U. Choi, A. Konarov, H. Yashiro, S. Yuan, L. Shi, Y.-K. Sun, S.-T. Myung, *Adv. Funct. Mater.* **2018**, *28*, 1705968.
[71] J. Jiao, K. Wu, R. Dang, N. Li, X. Deng, X. Liu, Z. Hu, X. Xiao, *Electrochim. Acta.* **2021**, *384*, 138362.
[72] Y.-S. Park, E.-S. Oh, S.-M. Lee, *J. Power Sources* **2014**, *248*, 1191.
[73] K. Ui, S. Kikuchi, F. Mikami, Y. Kadoma, N. Kumagai, *J. Power Sources* **2007**, *173*, 518.
[74] S. Komaba, K. Shimomura, N. Yabuuchi, T. Ozeki, H. Yui, K. Konno, *J. Phys. Chem. C* **2011**, *115*, 13487.
[75] S. V. Ebadi, A. Fakhrali, S. O. Ranaei-Siadat, A. A. Gharehaghaji, S. Mazinani, M. Dinari, J. Harati, *RSC Adv.* **2015**, *5*, 42572.
[76] J. Zhang, A. R. Horrocks, M. E. Hall, *Fire Mater.* **1994**, *18*, 307.
[77] K.-S. Lim, S.-T. Bee, L. T. Sin, T.-T. Tee, C. T. Ratnam, D. Hui, A. R. Rahmat, *Compos. B. Eng.* **2016**, *84*, 155.
[78] S. Roberts, L. Chen, B. Kishore, C. E. J. Dancer, M. J. H. Simmons, E. Kendrick, *J. Colloid Interface Sci.* **2022**, *627*, 427.
[79] J. Song, M. Zhou, R. Yi, T. Xu, M. L. Gordin, D. Tang, Z. Yu, M. Regula, D. Wang, *Adv. Funct. Mater.* **2014**, *24*, 5904.
[80] L. Qiu, Z. Shao, D. Wang, F. Wang, W. Wang, J. Wang, *Cellulose* **2014**, *21*, 2789.
[81] N. Jaikrajang, W. Kao-Ian, T. Muramatsu, R. Chanajaree, T. Yonezawa, Z. Y. Al Balushi, S. Kheawhom, R. Cheacharoen, *ACS Appl. Energy Mater.* **2021**, *4*, 7138.
[82] U. S. Vogl, P. K. Das, A. Z. Weber, M. Winter, R. Kostecki, S. F. Lux, *Langmuir* **2014**, *30*, 10299.
[83] H. Liu, X. Cheng, Y. Chong, H. Yuan, J. Q. Huang, Q. Zhang, *Particuology* **2021**, *57*, 56.
[84] G. Fourche, *Polym. Eng. Sci.* **1995**, *35*, 957.
[85] Y. Wang, J. Zhu, A. Chen, X. Guo, H. Cui, Z. Chen, Y. Hou, Z. Huang, D. Wang, G. Liang, S. C. Cao, C. Zhi, *Adv. Mater.* **2023**, *35*, 2303165
[86] I. Kovalenko, B. Zdyrko, A. Magasinski, B. Hertzberg, Z. Milicev, R. Burtovyy, I. Luzinov, G. Yushin, *Science* **2011**, 334.
[87] I. Dueramae, M. Okhawilai, P. Kasemsiri, H. Uyama, R. Kita, *Sci. Rep.* **2020**, *10*, 12587.
[88] R. Liutyi, I. Petryk, M. Tyshkovets, O. Myslyvchenko, D. Liuta, M. Fyodorov, *Adv. Ind. Manuf. Eng.* **2022**, *4*, 100082.
[89] Y. Orikasa, Y. Gogyo, H. Yamashige, M. Katayama, K. Chen, T. Mori, K. Yamamoto, T. Masese, Y. Inada, T. Ohta, Z. Siroma, S. Kato, H. Kinoshita, H. Arai, Z. Ogumi, Y. Uchimoto, *Sci. Rep.* **2016**, *6*, 26382.
[90] A. M. Bates, Y. Preger, L. Torres-Castro, K. L. Harrison, S. J. Harris, J. Hewson, *Joule* **2022**, *6*, 742.
[91] Y. Kuang, C. Chen, D. Kirsch, L. Hu, *Adv. Energy Mater.* **2019**, 9.
[92] B. Wang, J. Liu, Q. Sun, R. Li, T.-K. Sham, X. Sun, *Nanotechnology* **2014**, *25*, 504007.
[93] J. B. Bates, N. J. Dudney, G. R. Gruzalski, R. A. Zuhr, A. Choudhury, C. F. Luck, J. D. Robertson, *J. Power Sources* **1993**, *43*, 103.
[94] B. Wang, B. C. Chakoumakos, B. C. Sales, B. S. Kwak, J. B. Bates, *J. Solid State Chem.* **1995**, *115*, 313.
[95] E. Quérel, I. D. Seymour, A. Cavallaro, Q. Ma, F. Tietz, A. Aguadero, *JPhys Energy* **2021**, *3*, 044007.
[96] A. Hooper, P. Mcgeehin, K. T. Harrison, B. C. Tofield, *J. Solid State Chem.* **1978**, *24*, 265.
[97] O. E. O. Zeman, V. Kainz, T. Bräuniger, *Crystals* **2020**, *10*, 302.
[98] R. Blinc, J. Pirs, *J. Chem. Phys.* **1971**, *54*, 1535.
[99] J. Jung Kweon, K. Won Lee, C. Eui Lee, K.-S. Lee, Y. J. Jo, *Appl. Phys. Lett.* **2012**, *101*, 012905.
[100] R. Dang, M. Chen, Q. Li, K. Wu, Y. L. Lee, Z. Hu, X. Xiao, *ACS Appl. Mater. Interfaces* **2019**, *11*, 856.
[101] N. J. Garci?A, M. D. Ingram, J. C. Bazán, *Solid State Ion* **2002**, *146*, 113.
[102] J. Molinelli, M. Tomozawa, M. Takata, *J. Am. Ceram. Soc.* **1985**, *68*, 165.
[103] A. Nakagawa, N. Kuwata, Y. Matsuda, J. Kawamura, *J. Phys. Soc. Japan* **2010**, *79*, 98.
[104] E. Zhao, X. Liu, H. Zhao, X. Xiao, Z. Hu, *Chem. Comm.* **2015**, *51*, 9093.
[105] J. Janek, W. G. Zeier, *Nat. Energy* **2016**, *1*, 16141.
[106] H. Huo, J. Janek, *Natl. Sci. Rev.* **2023**, *10*, nwad098.
[107] Y.-K. Sun, *ACS Energy Lett.* **2020**, *5*, 3221.
[108] Y. Kato, S. Hori, R. Kanno, *Adv. Energy Mater.* **2020**, *10*, 2002153.
[109] S. Wenzel, S. Randau, T. Leichtweiß, D. A. Weber, J. Sann, W. G. Zeier, J. Janek, *Chem. Mater.* **2016**, *28*, 2400.
[110] P. Hartmann, T. Leichtweiss, M. R. Busche, M. Schneider, M. Reich, J. Sann, P. Adelhelm, J. Janek, *J. Phys. Chem. C* **2013**, *117*, 21064.
[111] S. Lou, F. Zhang, C. Fu, M. Chen, Y. Ma, G. Yin, J. Wang, *Adv. Mater.* **2021**, *33*, 2000721.
[112] Z. Jiang, Q. Han, S. Wang, H. Wang, *ChemElectroChem* **2019**, *6*, 2970.
[113] Z. Ding, J. Li, J. Li, C. An, *J. Electrochem. Soc.* **2020**, *167*, 070541.

[114] N. Boaretto, I. Garbayo, S. Valiyaveettil-Sobhanraj, A. Quintela, C. Li, M. Casas-Cabanas, F. Aguesse, *J. Power Sources* **2021**, *502*, 229919.
[115] S. Wang, R. Fang, Y. Li, Y. Liu, C. Xin, F. H. Richter, C.-W. Nan, *J. Mater.* **2021**, *7*, 209.
[116] K. T. Kim, D. Y. Oh, S. Jun, Y. B. Song, T. Y. Kwon, Y. Han, Y. S. Jung, *Adv. Energy Mater.* **2021**, *11*, 2003766.
[117] K. Lee, J. Lee, S. Choi, K. Char, J. W. Choi, *ACS Energy Lett.* **2019**, *4*, 94.
[118] D. Y. Oh, K. T. Kim, S. H. Jung, D. H. Kim, S. Jun, S. Jeoung, H. R. Moon, Y. S. Jung, *Mater. Today* **2022**, *53*, 7.
[119] S.-B. Hong, Y.-J. Lee, U.-H. Kim, C. Bak, Y. M. Lee, W. Cho, H. J. Hah, Y.-K. Sun, D.-W. Kim, *ACS Energy Lett.* **2022**, *7*, 1092.
[120] D. O. Shin, H. Kim, S. Jung, S. Byun, J. Choi, M. P. Kim, J. Y. Kim, S. H. Kang, Y.-S. Park, S. Y. Hong, M. Cho, Y.-G. Lee, K. Cho, Y. M. Lee, *Energy Storage Mater.* **2022**, *49*, 481.
[121] I. El Moctar, Q. Ni, Y. Bai, F. Wu, C. Wu, *Funct. Mater. Lett.* **2018**, *11*, 1830003.
[122] L. Xie, C. Tang, Z. Bi, M. Song, Y. Fan, C. Yan, X. Li, F. Su, Q. Zhang, C. Chen, *Adv. Energy Mater.* **2021**, *11*, 2101650.
[123] D. Hu, L. Chen, J. Tian, Y. Su, N. Li, G. Chen, Y. Hu, Y. Dou, S. Chen, F. Wu, *Chin. J. Chem.* **2021**, *39*, 165.
[124] Y. Liu, Y. M. Wang, B. I. Yakobson, B. C. Wood, *Phys. Rev. Lett.* **2014**, *113*, 028304.
[125] J.-T. Li, Z.-Y. Wu, Y.-Q. Lu, Y. Zhou, Q.-S. Huang, L. Huang, S.-G. Sun, *Adv. Energy Mater.* **2017**, *7*, 1701185.
[126] J. Zhao, X. Yang, Y. Yao, Y. Gao, Y. Sui, B. Zou, H. Ehrenberg, G. Chen, F. Du, *Adv. Sci.* **2018**, *5*, 1700768.
[127] H. Yamamoto, H. Mori, in *Lithium-Ion Batteries*, Springer, New York, NY **2009**, p. 163.
[128] J. Jin, Y. Liu, Q. Shen, X. Zhao, J. Zhang, Y. Song, T. Li, X. Xing, J. Chen, *Adv. Funct. Mater.* **2022**, *32*, 2203424.
[129] W. Zuo, J. Qiu, X. Liu, F. Ren, H. Liu, H. He, C. Luo, J. Li, G. F. Ortiz, H. Duan, J. Liu, M. S. Wang, Y. Li, R. Fu, Y. Yang, *Nat. Commun.* **2020**, *11*, 3544.
[130] T. Ma, G.-L. Xu, Y. Li, L. Wang, X. He, J. Zheng, J. Liu, M. H. Engelhard, P. Zapol, L. A. Curtiss, J. Jorne, K. Amine, Z. Chen, *J. Phys. Chem. Lett.* **2017**, *8*, 1072.
[131] M. Kuenzel, D. Bresser, T. Diemant, D. V. Carvalho, G.-T. Kim, R. J. Behm, S. Passerini, *ChemSusChem* **2018**, *11*, 504.
[132] I. Doberdò, N. Löffler, N. Laszczynski, D. Cericola, N. Penazzi, S. Bodoardo, G.-T. Kim, S. Passerini, *J. Power Sources* **2014**, *248*, 1000.
[133] A. Gabryelczyk, S. Ivanov, A. Bund, G. Lota, *J. Energy Storage* **2021**, *43*, 103226.
[134] V. Pamidi, C. Naranjo, S. Fuchs, H. Stein, T. Diemant, Y. Li, J. Biskupek, U. Kaiser, S. Dinda, A. Reupert, S. Behara, Y. Hu, S. Trivedi, A. R. Munnangi, P. Barpanda, M. Fichtner, Single crystal P2-$Na_{0.67}Mn_{0.67}Ni_{0.33}O_2$ cathode material with improved cycling stability for sodium ion batteries, (under review).
[135] C. Milroy, A. Manthiram, *Adv. Mater.* **2016**, *28*, 9744.
[136] F. Liu, Z. Hu, J. Xue, H. Huo, J. Zhou, L. Li, *RSC Adv.* **2019**, *9*, 40471.
[137] J. Zhang, M. Li, H. A. Younus, B. Wang, Q. Weng, Y. Zhang, S. Zhang, *Nano Mater. Sci.* **2021**, *3*, 124.
[138] Y. Zhou, L. Li, Y. Wu, H. Xie, *Eur. J. Inorg. Chem.* **2023**, *26*, 202200685.
[139] Z. Chen, Y. Qin, K. Amine, Y.-K. Sun, *J. Mater. Chem.* **2010**, *20*, 7606.
[140] H. Z. Zhang, Q. Q. Qiao, G. R. Li, X. P. Gao, *J. Mater. Chem. A* **2014**, *2*, 7454.
[141] Z.-F. Tang, R. Wu, P.-F. Huang, Q.-S. Wang, C.-H. Chen, *J. Alloys Compd.* **2017**, *693*, 1157.
[142] M. Chaudhary, S. Tyagi, R. K. Gupta, B. P. Singh, R. Singhal, *Surf. Coat. Technol.* **2021**, *412*, 127009.
[143] W. Li, Z. Yao, S. Zhang, X. Wang, X. Xia, C. Gu, J. Tu, *J. Chem. Eng.* **2021**, *421*, 127788.
[144] J. Lamb, A. Manthiram, *ACS Appl. Energy Mater.* **2021**, *4*, 11735.
[145] Y. Su, F. Yuan, L. Chen, Y. Lu, J. Dong, Y. Fang, S. Chen, F. Wu, *J. Energy Chem.* **2020**, *51*, 39.
[146] K. Sun, S. J. Dillon, *Electrochem. Commun.* **2011**, *13*, 200.
[147] X. Bian, Q. Fu, X. Bie, P. Yang, H. Qiu, Q. Pang, G. Chen, F. Du, Y. Wei, *Electrochim. Acta* **2015**, *174*, 875.
[148] S.-W. Lee, M.-S. Kim, J. H. Jeong, D.-H. Kim, K. Y. Chung, K. C. Roh, K.-B. Kim, *J. Power Sources* **2017**, *360*, 206.
[149] X. Li, R. Yang, B. Cheng, Q. Hao, H. Xu, J. Yang, Y. Qian, *Mater. Lett.* **2012**, *66*, 168.
[150] S.-X. Zhao, H. Ding, Y.-C. Wang, B.-H. Li, C.-W. Nan, *J. Alloys Compd.* **2013**, *566*, 206.
[151] B. Wang, J. Liu, M. Norouzi Banis, Q. Sun, Y. Zhao, R. Li, T.-K. Sham, X. Sun, *ACS Appl. Mater. Interfaces* **2017**, *9*, 31786.
[152] Q. Zhang, W. Jiang, Z. Zhou, S. Wang, X. Guo, S. Zhao, G. Ma, *Solid State Ion* **2012**, *218*, 31.
[153] S. Yang, W. Ren, J. Chen, *Front. Energy* **2017**, *11*, 374.
[154] S. Liu, H. Wu, L. Huang, M. Xiang, H. Liu, Y. Zhang, *J. Alloys Compd.* **2016**, *674*, 447.
[155] N. Chebaeva, M. Lettner, J. Wenger, J.-P. Schöggl, F. Hesser, D. Holzer, T. Stern, *J. Clean. Prod.* **2021**, *281*, 125232.
[156] R. K. Singh, H. R. Murty, S. K. Gupta, A. K. Dikshit, *Ecol. Indic.* **2009**, *9*, 189.
[157] D. B. Agusdinata, W. Liu, H. Eakin, H. Romero, *Environ. Res. Lett.* **2018**, *13*, 123001.
[158] A. Leader, G. Gaustad, C. Babbitt, *Mater. Renew. Sustain Energy* **2019**, *8*, 8.
[159] M. Erakca, S. Pinto Bautista, S. Moghaddas, M. Baumann, W. Bauer, L. Leuthner, M. Weil, *J. Clean. Prod.* **2023**, *384*, 135510.
[160] F. Arshad, J. Lin, N. Manurkar, E. Fan, A. Ahmad, M.-U.-N. Tariq, F. Wu, R. Chen, L. Li, *Resour. Conserv. Recycl.* **2022**, *180*, 106164.
[161] G. Rodriguez-Garcia, J. Braun, J. Peters, M. Weil, *Matér. Techn.* **2017**, *105*, 517.
[162] F. Gschwind, G. Rodriguez-Garcia, D. J. S. Sandbeck, A. Gross, M. Weil, M. Fichtner, N. Hörmann, *J. Fluor. Chem.* **2016**, *182*, 76.
[163] European Commission 2008, EC 2008 Regulation (EC) No 1272/2008 of the European Parliament and of the Council of 16 December 2008, (EC) No 1907/2006.
[164] https://echa.europa.eu/SCOEL/SUM/119 (accessed: August 2007).
[165] D. L. Wood, J. D. Quass, J. Li, S. Ahmed, D. Ventola, C. Daniel, *Dry. Technol.* **2018**, *36*, 234.
[166] S. Havelange, N. Lierde, A. Germeau, E. Martins, T. Theys, M. Sonveaux, C. Toussaint, K. Schrödter, G. Bettermann, T. Staffel, F. Wahl, T. Klein, T. Hofmann, in *Ullmann's Encycl. Ind. Chem.*, Wiley, Hoboken, NJ **2022**, 1.
[167] R. S. Lanigan, *Int. J. Toxicol.* **2001**, *20*, 75.
[168] R. Lohmann, I. T. Cousins, J. C. Dewitt, J. Glüge, G. Goldenman, D. Herzke, A. B. Lindstrom, M. F. Miller, C. A. Ng, S. Patton, M. Scheringer, X. Trier, Z. Wang, *Environ. Sci. Technol.* **2020**, *54*, 12820.

Shivam Trivedi is presently a doctoral student at the Helmholtz Institute Ulm (HIU). He worked on inorganic aqueous binders and authored several publications in this area. Prior to this, he held several positions as research staff in the area of electrochemical energy storage and layered materials.

Venkat Pamidi is a battery materials scientist at Faradion, UK. He obtained his Ph.D. in sodium-ion batteries investigating single crystalline cathodes and inorganic binders. He also gained research experience in similar areas after a Master's degree in materials engineering.

Sebastian Pinto Bautista is a Ph.D. candidate at the Institute for Technology Assessment and Systems Analysis (ITAS). He specialized in Life Cycle Analysis after concluding his studies in Sustainable Systems Engineering and currently focuses on evaluating the sustainability profile of energy.

Farra Nur Aliah Binti Shamsudin is a Master's student at the Technical University Ingolstadt of Applied Sciences. She obtained her Bachelor's degree at the University of Applied Sciences Merseburg and focused her Bachelor's thesis on the evaluation of the environmental profile of inorganic binders via the life cycle assessment (LCA) method and the hazard level assessment.

Marcel Weil is a research group leader at ITAS and HIU at KIT and chairman of the Task Force Sustainability, a joint activity of BEPA and Batteries Europe. He is also on the board of directors of the Cluster of Excellence for Post-Lithium Batteries (POLiS). He received his doctorate from TU-Darmstadt after which he held several scientific positions at KIT. He has authored >150 publications (h index:33).

Prabeer Barpanda is an associate professor at the Indian Institute of Science, India. He obtained his Ph.D. from Rutgers University, USA and then pursued post-doctoral work at the Université de Picardie Jules Verne in France and the University of Tokyo, Japan. His work revolves around synthesis, structure, and electrochemical investigations for secondary Li-ion and post-Li-ion batteries.

Dominic Bresser is serving as group leader and principal investigator at HIU/KIT in Germany. Prior to this, he completed his Ph.D. at the University of Muenster, Germany and held a postdoctoral position at CEA in Grenoble, France. His research focuses on new and optimized electrode materials, electrolytes, and electrode preparation processes for lithium and sodium batteries. He has co-authored >170 publications (h-index: 48) and >20 patents and patent applications in the field of electrochemical energy storage.

Maximilian Fichtner is a professor of solid-state chemistry at Ulm University, director at HIU, and spokesman of the Cluster of Excellence POLiS. He is also the head of the Department "Energy Storage Systems" at the Institute of Technology (INT), KIT. He has authored >400 scientific publications (h-index:70) in the area of energy storage.